이학박사 학위논문

Variational approach for image segmentation incorporating shape knowledge

(형태 지식을 사용한 영상 분할을 위한 변분법적 접근)

2014년 8월

서울대학교 대학원

수리과학부

둘투야

Variational approach for image segmentation incorporating shape knowledge

A dissertation
submitted in partial fulfillment
of the requirements for the degree of
Doctor of Philosophy
to the faculty of the Graduate School of
Seoul National University

by

Dultuya Terbish

Dissertation Director : Professor Myungjoo Kang

Department of Mathematical Sciences
Seoul National University

August 2014

Abstract

In this dissertation, we discuss segmentation algorithms based on the level set method that incorporates shape prior knowledge. Fundamental segmentation models fail to segment desirable objects from a background when the objects are occluded by others or missing parts of their whole. To overcome these difficulties, we incorporate shape prior knowledge into a new segmentation energy that, uses global and local image information to construct the energy functional. This method improves upon other methods found in the literature and segments images with intensity inhomogeneity, even when images have missing or misleading information due to occlusions, noise, or low-contrast. We consider the case when the shape prior is placed exactly at the locations of the desired objects and the case when the shape prior is placed at arbitrary locations. We test our methods on various images and compare them to other existing methods. Experimental results show that our methods are not only accurate and computationally efficient, but faster than existing methods as well.

Key words: Segmentation, active contours, shape prior knowledge, level set method, intensity inhomogeneity
Student Number: 2010-31290

Contents

List of Figures

LIST OF FIGURES

List of Tables

Chapter 1

Introduction

1.1 Research background

Image segmentation is one of the most basic concepts in image processing. Extensive research on this topic has produced a numerous of segmentation methods. The goal of image segmentation is to partition an image into regions of objects detected from background of the image. The choice of a segmentation method depends on the properties of the image.

Most segmentation approaches are based on the Mumford-Shah (MS) functional [1], which is a region based model. Another common approach is the active contour model, which is an edge based model. This model detects significant contours rather than partitioning an image into homogeneous regions. Other traditional approaches are discussed in [16, 17, 19]. Even though these models are capable of detecting objects in an image, they fail to detect an object's interior. Furthermore, once a curve(or contour) detects an object's boundary, segmentation stops.

To overcome the drawbacks of traditional approaches [16, 17, 19], Chan and Vese (Chan-Vese) propose one of the well-known approach named active contours without edges [2], and reformulate the MS functional in terms of the level set method [3]. This approach was also extended to images with multiple-regions [4]; however, the re-initialization process of

the level set functions makes it computationally expensive. In this extension, they proposed the piecewise constant (PC) model, which works well on the images with intensity homogeneity and the piecewise smooth (PS) approach, which segments images with intensity inhomogeneity. Unfortunately, these methods are computationally expensive as well.

Inspired by the active contour model, the local binary fitting (LBF) method was proposed to segment images with intensity inhomogeneity [11, 12]. This method imposes local intensity information as constraints and eliminates the re-initialization process by using *variational level set formulation without re-initialization* [36, 37]. The LBF method produces better segmentation results and is more computationally efficient than the PS model. The local image fitting (LIF) energy approach was also designed of the LBF model and to regularize the level set function using Gaussian filtering for variational level set; thus, LIF eliminates the re-initialization process.

All of these methods fail to segment images with missing or misleading information due to occlusion, noise or low-contrast. Therefore, shape prior knowledge is incorporated to improve the robustness of such segmentation methods. Many approaches have been developed for shape prior segmentation. In general, the segmentation methods that incorporate shape information can be classified into two types:

1. Based on statistical knowledge of the shape [5–7, 29, 30, 35].

    - This method uses a set of training shapes to create a mean shape. Training set points are aligned to minimize the weighted sum of squares of the distances between equivalent points on different shapes. The mean shape evolves to fit the object to be segmented. To achieve better segmentation results, statistical tools, such as mean value and principal component analysis are used.

2. Based on level set knowledge of the shape [8–10, 18, 26–28, 31, 34].

- This method embeds the shape prior using the level set function. Topological changes, such as splitting and merging, allow several objects in a given image to be segmented.

We focus on the level set knowledge of the shape, which allows us to use a variational approach. Most methods focus on segmenting only one desired object, Cremers et al.'s model, on the other hand, can segment the desired object and others in a given image by introducing a labeling function [9]. In this model, the size, pose and location of the shape have to be similar to the desired one; in other words, geometric transformations of the shapes are prohibited. To overcome this limitation, Chan and Zhu proposed an algorithm [10] in which the shape term is independent of the image domain. An additional term enables the labeling function to be easily controlled. Thiruvenkadam et al. [27] and J. Woo et al. [28] extended the Chan-Zhu model to segment images with multiple-regions. These models are PC models; thus, they do not work well for the images with intensity inhomogeneity.

Inspired by Wang et al.'s model [13], we propose a segmentation method for images with intensity inhomogeneity by modifying the LIF model. Our model drives the motion of the contour far away from object boundaries by utilizing the fitting term of the Chan-Vese model as an auxiliary global intensity fitting term. Therefore, the initial level set is more flexible, and the computation cost is less than that of the LIF model.

Fundamental methods for shape prior segmentation utilize a general energy functional that is a linear combination of segmentation energy and shape energy. Analogous to the general energy functional, we minimize a total energy function that, consists of our modified LIF energy and the shape energy. Our approach is able to segment the desired object, as well as other objects, when images have independent intensity inhomogeneous and homogeneous regions. Moreover, our approach succeeds even when objects are occluded or missing some parts (i.e., the image is corrupted). We consider two cases for the location of given shape prior. First, the shape

prior is placed exactly at the locations of desired objects. Second, a given shape prior is placed at arbitrary locations. Numerical experiments show that our approach is more inexpensive and accurate than extensions of models proposed by Cremers et al. and Chan and Zhu.

1.2 Outline of thesis

This dissertation is organized as follows: Chapter 2 discusses previous works. We review image segmentation models for images with intensity homogeneity and inhomogeneity and review the shape prior segmentation models for images with noise, occlusions or low-contrast. The main contributions of this thesis are presented in Chapter 3. In Section 3.1, we propose a novel method for images with intensity inhomogeneity, named the active contours driven by global and local image fitting energy. In order to cope with the intensity inhomogeneity of the image, we set a local image fitting term. To overcome sensitivity of initialization, a global image fitting term is considered. In Section 3.2, we propose a shape prior segmentation, which incorporates shape prior knowledge to improve robustness and segment the multiple objects with different intensities using only one level set function. Numerical experiments are discussed in Chapter 4. Finally, we conclude our work in Chapter 5.

Chapter 2

Previous works

2.1 Level set method

The level set method is used to segment an image by evolving a curve to capture the objects. The basic idea is to represent contour as the zero level set of an implicit function defined in a higher dimension. The level set function is propagated by a partial differential equation (PDE). The main advantage of the level set method is that the zero level set can merge, break and change its topology during its evolution for segmentation problems (see Fig. 2.1).

The curves, denoted by C, are represented by a zero level set of an implicit function $\phi(t, x, y)$. Specifically,

$$C(t) = \{(x, y)|\phi(t, x, y) = 0\}.$$

The evolution equation of the level set function ϕ can be written as

$$\frac{\partial \phi}{\partial t} + F|\nabla \phi| = 0. \tag{2.1}$$

Equation (2.1) is called the "*level set equation*" in the traditional level set method [3]. The zero level set of $\phi(t, x, y)$ moves along at speed F, which depends on image data such as its edges.

The level set function (LSF) ϕ of traditional level set methods [3, 15, 20] creates shocks, very sharp or flat shapes during its evolution, which makes

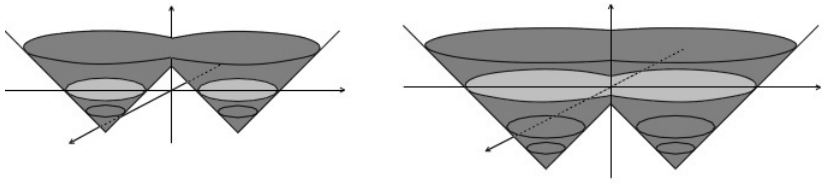

Figure 2.1: Change topology of the level set.

further computation highly inaccurate. To overcome these problems, the fundamental level set method initializes ϕ as a signed distance function (SDF) before evolution begins. In other words, the degraded level set function is periodically re-initialized (or reshaped) during its evolution.

The re-initialization process has been extensively investigated [20–23]. The classic re-initialization method solves the following equation:

$$\frac{\partial \phi}{\partial t} = sign(\phi_0)(1 - |\nabla \phi|) \tag{2.2}$$

where ϕ_0 is the function to be re-initialized, and $sign(\phi)$ is the sign function of ϕ defined by

$$sign(\phi) = \begin{cases} 1 & \text{if } \phi > 0 \\ 0 & \text{if } \phi = 0 \\ -1 & \text{if } \phi < 0. \end{cases}$$

The re-initialization process cannot be avoided, and it is complicated and expensive to use in practice. The most popular models, Geodesic Active Contours and the Chan-Vese Model, are based on traditional level set methods. These methods re-initialize the LSF using (2.2). We will discuss these segmentation methods in the next section.

Li et al. proposed a new variational level set formulation [36, 37] that avoids the re-initialization process. They further generalized their formulation by using a signed distance regularization term [37]. By definition, the SDF of the LSF must satisfy $|\nabla \phi| = 1$. Li et al. designed their formulation with

an intrinsic mechanism to maintain the signed distance property of the LSF [36]. This mechanism is associated with "a penalty term", which penalizes deviation of the LSF from the SDF. Therefore, the re-initialization process is eliminated, which results in a more efficient algorithm than the classical level set formulation.

The penalizing term in [37] is given by the following integral:

$$P(\phi) = \int_{\Omega} \frac{1}{2}(|\nabla\phi| - 1)^2 dxdy. \tag{2.3}$$

This integral can used to determine how close a function ϕ is to the SDF in $\Omega \subset R^2$. The penalizing term plays a key role in the variational level set formulation. Furthermore, (2.3) maintain the LSF as an approximate SDF during the evolution, especially in a neighborhood around the zero level set.

To explain the effects of the penalty term, the gradient flow is very useful. The gradient flow is given by

$$\frac{\partial\phi}{\partial t} = \Delta\phi - div\left(\frac{\nabla\phi}{|\nabla\phi|}\right) = div\left[(1 - \frac{1}{|\nabla\phi|})\nabla\phi\right]. \tag{2.4}$$

Properties of the SDF are evident in (2.4). Factor $(1 - \frac{1}{|\nabla\phi|})$ is the diffusion rate. The diffusion rate is positive, if $|\nabla\phi| > 1$; this term makes ϕ smoother, thereby reducing the gradient $|\nabla\phi|$. On the contrary, reverse diffusion occurs when $|\nabla\phi| < 1$; thus, in this case, the gradient increases. Therefore, the LSF automatically forced to be an approximate SDF during the evolution. Functional $P(\phi)$ is applied to an active contours algorithm for image segmentation. This concept is discussed in Section 2.3.

Zhang et al. [14] took a different approach and proposed the variational level set with Gaussian filtering. They were inspired by the fact that the evolution of a function, according to its Laplacian, is equivalent to Gaussian filtering the initial condition of the function. Furthermore, they noticed that, the previous iteration result of the level set function can be viewed as the initial condition for the next iteration, i.e.,

$$\phi^{n+1} = G_{\sqrt{\Delta t}} * \phi^n$$

where $G_{\sqrt{\Delta t}}$ is a Gaussian kernel with variance Δt, and $*$ is the convolution operator. This equation is a solution to the following equation at time $t = (n+1)\Delta t$:

$$\phi_t = \Delta\phi. \tag{2.5}$$

The initial condition is $\phi(x, t = n\Delta t) = \phi^2$, where n is the iteration number and Δt is the time-step.

To obtain the solution to (2.5), we first express ϕ^{n+1} as

$$\phi^{n+1} = \phi^n + \Delta t \Delta\phi^n \tag{2.6}$$

where Δt is the time-step. In general, clearly, (2.6) is not smooth because the Laplacian term is defined on a point-by-point basis, whereas the Gaussian filtering uses all the points around the center point to make the level set function smooth. Zhang et al. utilized this variational level set method in a new, region-based active contour model for images with intensity inhomogeneity. This will be described in more detail in Section 2.3.

2.2 Fundamental models for image segmentation

The first fundamental model for image segmentation was proposed by Mumford and Shah in 1989 [1]. Their main idea is to approximate an image by a simplified image as a combination of regions of constant intensities and the smoothness of the contours was disregarded. These ideas were incorporated into a variational framework; an initial image I_0, find pair (I, C), where I is a nearly piecewise smooth approximation of I_0 and C is the set of edges. Mumford and Shah proposed to find (I, C) by minimizing the following functional:

$$F^{MS}(I, C) = \int_{\Omega - C} (I - I_0)^2 dx + \alpha \int_{\Omega - C} |\nabla I|^2 dx + \beta \int_C d\sigma \qquad (2.7)$$

where Ω is a bounded open set of $\mathbb{R}^2$, α and β are nonnegative constants and $\int_C d\sigma$ is the length of C. We refer to (2.7) as the Mumford-Shah (MS) functional.

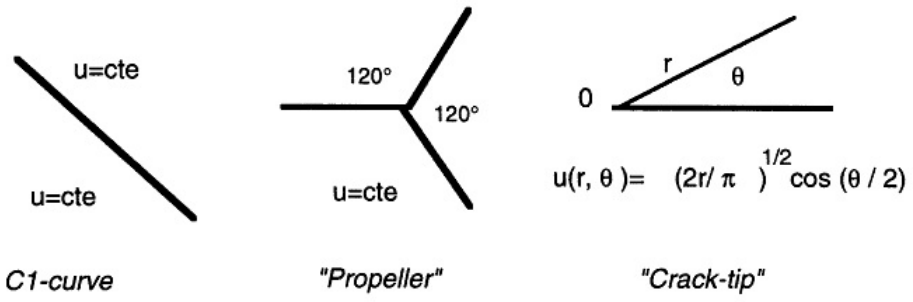

Figure 2.2: Local behaviour of curves

Furthermore, Mumford and Shah conjectured that *there exists a minimizer of F^{MS} such that the edges are the union of a finite set of $C^{1,1}$ embedded curves and that each curve ends in either a crack tip (a free extremity i.e., C looks like a half line) or triple junction.*

To examine the existence of a solution to the MS problem, they predicted the local behavior for the possible endpoints and crossings of curves as shown in Fig.2.2 and analyzed the conjecture. In practice, it is difficult to minimize the MS functional because dimension of C is unknown, and the problem is nonconvex. Theoretical results and the regularity of minimizers of (2.7) can be found in [1].

Methods of solving the general MS model are complicated and computationally expensive, even though, (2.7) is a natural method of segmentation. Therefore, Mumford and Shah formulated a reduced version of the MS functional called the *minimal partition problem*, which can be formulated as follows:

$$E^{MS}(I, C) = \sum_i \int_{\Omega_i} (I_0 - c_i)^2 dxdy + \beta \int_C d\sigma \tag{2.8}$$

The solution of the minimal partition problem can be found by restricting the segmented image I to a piecewise constant approximation I_0, i.e., $I = c_i$ in each connected component Ω_i, where c_i are constants. For fixed C, minimizing F^{MS} functional is reduced to minimize E^{MS} in variables c_i by setting $c_i = mean(I_0)$ in each Ω_i. However, minimizing the reduced MS functional is still very difficult due to its nonconvexity.

A wide variety of active contour based models have been reported in the existing research. The classic active contour model named "Snake" was proposed by Kass, Witkin, and Terzopoulos in 1987 [19]. Their goal was to detect contours of objects automatically. The Snake model raises two very important questions: how are contours represented, and what criteria allow one to select the true contours? To answer these questions, the following energy functional was proposed:

$$J_1^{Snake}(c) = \int_a^b |c'(x)|^2 dx + \beta \int_a^b |c''(x)|^2 dx + \lambda \int_a^b g^2(|\nabla I(c(x))|) dx \tag{2.9}$$

where C is the set of curves in $\mathbb{R}^2$ defined by

$$C = \{c : [a, b] \to \Omega,\ c \text{ piecewise } C^1,\ c(a) = c(b)\}.$$

The first two terms in (2.9) are the internal energy. Curve c makes the snake act like a membrane and thin plate when the energy is minimized. The third term is the external energy that pulls the curve toward the edges of the objects.

Because of the magnitude of the gradient of image I is high across the boundaries of objects, $|\nabla I(x,y)| = \sqrt{I_x^2 + I_y^2}$ is chosen as a detector for contours. In order to characterize edges by zero values rather than infinite values, Kass, Witkin, and Terzopoulos defined the edge detector function $g : [0, +\infty[\rightarrow]0, +\infty[$. This function is regular, monotonic, and decreasing; it also has the properties that $g(0) = 1$ and $\lim_{x \rightarrow +\infty} g(x) = 0$. A typical choice of g is $g(\nabla I) = 1/(1 + |\nabla I|^2)$. Figure 2.3 shows an example of an edge detector function. The edges of the image can clearly be distinguished.

Figure 2.3: Original house image (left), result of $\nabla I(x,y)$ (middle), and result of $g(\nabla I)$ (right).

Using calculus of variations, a global solution to (2.9) can be found. Since Ω is bounded, the Euler-Lagrange equation associated with $J_1^{snake}(c)$ in the Sobolev space $(W^{2,2}(a,b))^2$ can be solved. Uniqueness, however, is not guaranteed since $J_1^{snake}(c)$ is nonconvex. Other disadvantages associated with the Snake model are: 1)$J_1^{snake}(c)$ is not intrinsic because it depends on the parametrization of c; thus, it is called parametric active contours, 2) the regularity constraint prohibits the model from handling changes in topology, 3) if the initial curve does not surround the object, false detections may occurs, 4) it does not allow for flexible initialization of the

curve.

To overcome the disadvantages of the Snake model, the Geodesic Active Contours model was proposed by Caselles et al. in 1997 [17]. They modified J_1^{snake} when $\beta = 0$ as follows:

$$J_2^{GAC}(c) = 2\sqrt{\lambda} \int_a^b g(|\nabla I(\bar{c}(s))|)|\bar{c}'(s)|ds$$

where $\bar{c}(s) = c(\phi(s))$. This model can be thought of as a weighted Euclidean length, with weight $g(|\nabla I(\bar{c}(s))|)$, which includes information concerning the boundaries (edges) of desired objects. This method is geometrically intrinsic because it does not depend on the parametrization of curve c.

Again, using calculus of variations and the steepest descent method, the gradient descent flow is given by

$$\frac{\partial c}{\partial t} = (kg - \langle \nabla g, N \rangle + \alpha g)N \tag{2.10}$$

for an initial curve $c_0(x)$. Here, k is the curvature, and N is the normal to curve C. The main advantage of Casseles et al.'s model is its level set expression. They proposed an intrinsic model motivated by the level set method in [3]. The level set formulation of (2.10) can be written as

$$\frac{\partial \phi}{\partial t} = g(|\nabla I|) \left(\text{div} \left(\frac{\nabla \phi}{|\nabla \phi|} \right) + \alpha \right) |\nabla \phi| + \langle \nabla g, \nabla \phi \rangle \tag{2.11}$$

for given boundary and initial conditions.

By applying the level set method, implementation of (2.11) is made significantly easier. In (2.11), $g(|\nabla I|)$ permits one to stop the evolving curve when it arrives at an object's boundary, and $\langle \nabla g, \nabla \phi \rangle$ increases the attraction of the deforming contour toward the object boundaries. While this method improves upon the Snake model, the interior of objects cannot segmented, i.e., once the curve has detected a contour, it stops. Furthermore, this method is computationally expensive because it requires re-initialization during the evolution of the LSF.

A region-based segmentation method with level sets was proposed by Chan and Vese [2, 24]. This is a variational approach for image segmentation without a terminating edge-function, i.e., the model does not include the gradient of the image to stop the process. Moreover, it can automatically detect the interior contours of objects using flexible initial curve. The Chan-Vese model is a particular case of the MS segmentation technique when i=2. Chan and Vese proposed minimizing the following functional:

$$E^{Chan-Vese}(c_1, c_2, C) = \lambda_1 \int_{in(C)} |I_0 - c_1|^2 dx + \lambda_2 \int_{out(C)} |I_0 - c_2|^2 dx + \mu \cdot \text{Length}(C) + \nu \cdot \text{Area(inside(C))} \tag{2.12}$$

where I_0 is a given image on the bounded open subset Ω in $\mathbb{R}^2$. In most cases, $\nu = 0$ and $\lambda_1 = \lambda_2 = 1$. The sum of the first and second integrals in (2.12) is called the fitting term/stopping term. That is,

$$E^{fitting}(C) = F_{in}(C) + F_{out}(C) = \int_{in(C)} |I_0 - c_1|^2 dx + \int_{out(C)} |I_0 - c_2|^2 dx.$$

A visual explanation of the fitting term is illustrated in Fig.2.4. In this figure, $F_{in}(C) \approx 0$ and $F_{out}(C) > 0$ when curve C is inside the object. On the other hand, $F_{in}(C) > 0$ and $F_{out}(C) \approx 0$ when C is outside the object. If C is both inside and outside the object, $F_{in}(C) > 0$ and $F_{out}(C) > 0$. On the contrary, $F_{in}(C) \approx 0$ and $F_{out}(C) \approx 0$ when $E^{fitting}(C)$ is minimized.

Curve $C \subset \Omega$ can be expressed implicitly by a zero level set of $\phi : \Omega \to R$:

$$\begin{cases} C = \{(x, y) \in \Omega : \phi(x, y) = 0\} \\ in(C) = inside(C) = \{(x, y) \in \Omega : \phi(x, y) > 0\} \\ out(C) = outside(C) = \{(x, y) \in \Omega : \phi(x, y) < 0\}. \end{cases} \tag{2.13}$$

Using the zero level set function ϕ, the terms of the Chan-Vese energy,

(a) (b)

(c) (d)

Figure 2.4: Explanation of the fitting term: $F_{in}(C) \approx 0$ and $F_{out}(C) > 0$ when curve C is inside the object (a), $F_{in}(C) > 0$ and $F_{out}(C) \approx 0$ when curve C is outside the object (b), If curve C is both inside and outside the object, $F_{in}(C) > 0$ and $F_{out}(C) > 0$ (c), On the contrary, $F_{in}(C) \approx 0$ and $F_{out}(C) \approx 0$ when $E^{fitting}$ is minimized (d).

$E^{Chan-Vese}$ can be represented as follows:

$$Length\{\phi = 0\} = \int_{\Omega} |\nabla H(\phi(x,y))| dxdy = \int_{\Omega} \delta_0(\phi(x,y)) |\nabla \phi(x,y)| dxdy,$$

$$Area\{\phi \geq 0\} = \int_{\Omega} H(\phi(x,y)) dxdy$$

and

$$F_{in}(C) = \int\limits_{\phi>0} |I_0(x,y) - c_1|^2 dxdy = \int\limits_{\Omega} |I_0(x,y) - c_1|^2 H(\phi(x,y))dxdy,$$
$$F_{out}(C) = \int\limits_{\phi<0} |I_0(x,y) - c_2|^2 dxdy = \int\limits_{\Omega} |I_0(x,y) - c_2|^2 (1 - H(\phi(x,y)))dxdy.$$

where

$$H(\phi) = \begin{cases} 1, \text{if } \phi \geq 0 \\ 0, \text{if } \phi < 0 \end{cases}, \ \delta_0(\phi) = \frac{d}{d\phi} H(\phi).$$

As a result, the level set formulation of $E^{Chan-Vese}$ can be written as

$$\begin{aligned} E^{Chan-Vese}(c_1, c_2, \phi) = &\int_{\Omega} ((I_0 - c_1)^2 H(\phi) + (I_0 - c_2)^2 (1 - H(\phi)))dx \\ &+ \mu \int_{\Omega} |\nabla H(\phi)|dx + \nu \int_{\Omega} H(\phi)dx. \end{aligned} \tag{2.14}$$

As shown in Fig.(2.5), the curve of the Geodesic Active Contour model cannot detect the interior boundary of objects. Also, if the initial level set is not surrounded, object detection fails as shown in Figs.2.5(b) and (2.5)(e). This is not a problem for the Chan-Vese model, however Fig.2.5(f) and initialization does not depend on position Fig.2.5(c).

Inspired by Zhao et al. [38], Vese and Chan extended their model using a multiphase level set formulation to partition multiple regions. Piecewise constant(PC) and Piecewise smooth(PS) models were proposed in [4]. For the PC model, level set functions $\phi_i : \Omega \to R$, $i = 1, ..., m$ were considered. The union of the zero-level sets of ϕ_i represent the contours in the segmented image. The segments, or phases, in domain Ω can be defined as follows:

Proposition 2.2.1. *Two pixels (x_1, y_1) and (x_2, y_2) in Ω belong to the same phase, or class, if and only if $H(\Phi(x_1, y_1)) = H(\Phi(x_2, y_2))$. Here, $\Phi = (\phi_1, ..., \phi_m)$ is the vector of level set functions and $H(\Phi) = (H(\phi_1), ..., H(\phi_m))$ is the vector of Heaviside functions whose components are 1 or 0.*

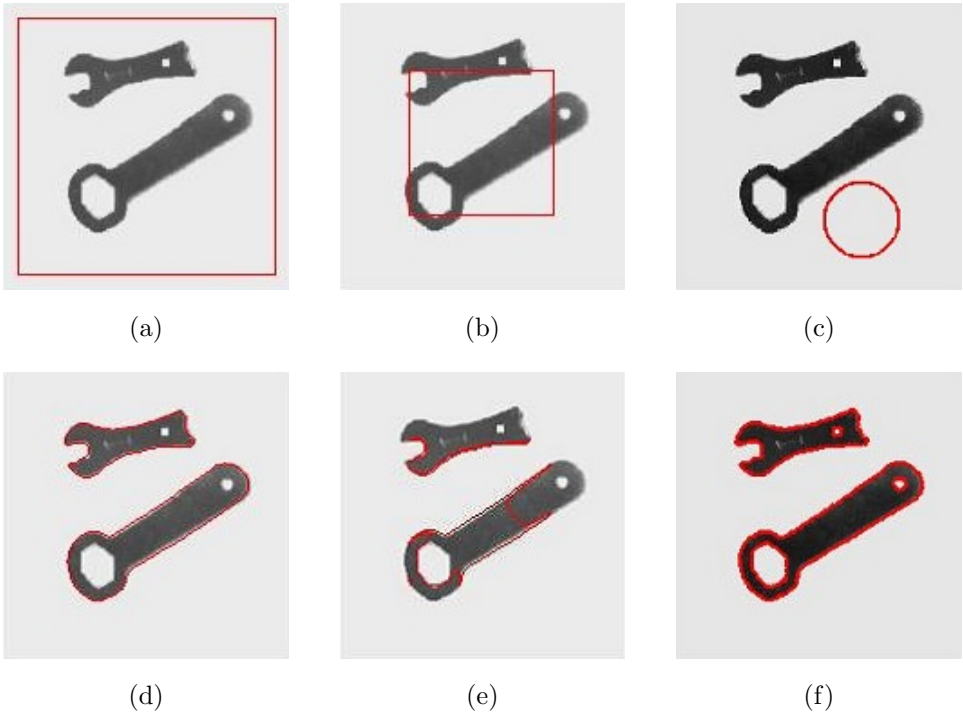

(a) (b) (c)

(d) (e) (f)

Figure 2.5: Segmentation results of the Geodesic Active Contour and Chan-Vese models

Up to $n = 2^m$ phases or classes can be defined in the domain of definition Ω. Classes defined in this form a disjoint decomposition and covering of Ω. Therefore, each pixel $(x, y) \in \Omega$ belongs to only one class, and there is no vacuum or overlap among phases. The set of curves is represented by the union of the zero level sets of the functions ϕ_i.

As shown in Fig.(2.6), two level set functions ($m = 2$) are required to represent four phases ($n = 4$) in the PC model. Therefore, the energy of the four phase PC model can be written as:

$$E_4^{PC}(c, \Phi) = \sum_i^n \sum_j^m \int_\Omega ((I_0 - c_{i,j})^2 H_{i,j} dx + \int_\Omega |\nabla H(\phi_1)| + \int_\Omega |\nabla H(\phi_2)|$$

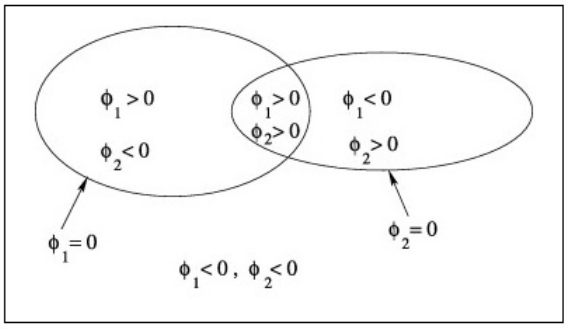

Figure 2.6: Four phases of two level set functions

where

$$H_{11} = H(\phi_1)H(\phi_2),\ H_{12} = H(\phi_1)(1 - H(\phi_2))$$
$$H_{21} = (1 - H(\phi_1))H(\phi_2),\ H_{22} = (1 - H(\phi_1))(1 - H(\phi_2))$$

and $c_{i,j} = \text{mean}(I_0)$, $(i = 1, 2,\ j = 1, 2)$ in each region/phase.

Figure 2.7 shows the segmentation results of a noisy synthetic image with a triple junction. Using only one level set function in the Chan-Vese model (Fig.2.7(a)), it is impossible to represent the triple junction (Fig.2.7(b)). If two level set functions are used (Fig.2.7(c)) by the PC model and $n = 4$, the triple junction can be represented, and four phases are extracted as shown in Fig.2.7(d).

The PC model has the advantage that it can represent triple junctions and multiple regions. The works of Chan and Vese have led to numerous segmentation methods. For example, Kim and Kang [40] proposed an efficient algorithm for multiple-region segmentation and considered finding the number of regions in a given image automatically. These methods work well for images with intensity homogeneity (or roughly constant in each phase) but do not work for images with intensity inhomogeneity. For images with intensity inhomogeneity, figure (2.8) shows an example of when object is unsuccessfully segmented. The Chan-Vese model does not perform well (Fig.2.8(c)). Methods for images with intensity inhomogeneity are discussed in the next section.

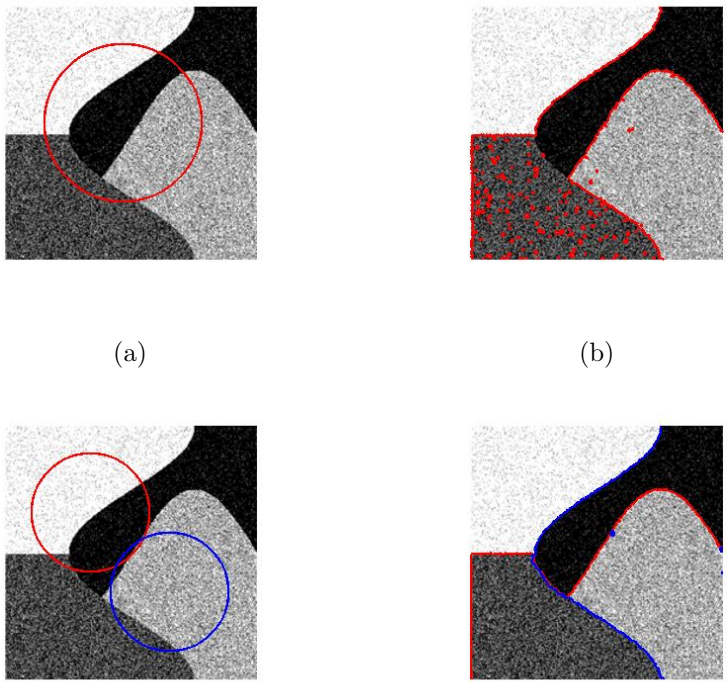

(a) (b)

(c) (d)

Figure 2.7: PC model segmentation results for an image with a triple junction

(a)

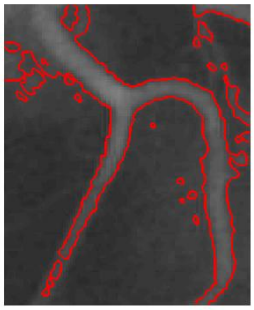

(b)

(c)

Figure 2.8: Segmentation results of the Chan-Vese model.

2.3 Segmentation models for images with intensity inhomogeneity

Intensity inhomogeneity often occurs as a result of technical limitations. In particular, inhomogeneities in magnetic resonance (MR) images arise from nonuniform magnetic fields produced by ratio-frequency coils, as well as from variations in object susceptibility. Therefore, many segmentation approaches have been developed for images with intensity inhomogeneity.

The first approach is a piecewise smooth (PS) model proposed by Vese and Chan [4]. Consider the PS model for images with intensity inhomogeneity when $n = 2$ (two phase case). The edges in the image can be represented by one level set function ϕ as

$$C = \{(x, y) \mid \phi(x, y) = 0\}.$$

Functions f^+ and f^- are assumed to be C^1 functions on $\phi \geq 0$ and $\phi \leq 0$ respectively. And the link between unknowns $f = f^+H(\phi) + f^-(1 - H(\phi))$ and ϕ can be expressed by introducing two functions f^+ and f^- such that

$$f(x, y) = \begin{cases} f^+(x, y), & \text{if } \phi(x, y) \geq 0 \\ f^-(x, y), & \text{if } \phi(x, y) < 0. \end{cases}$$

The PS model is formulated as minimizing the following energy:

$$E_2^{PS}(f^+, f^-, \Phi) = \int_\Omega ((I_0 - f^+)^2 H(\phi) + (I_0 - f^-)^2 (1 - H(\phi)))dxdy + \mu \int_\Omega (|\nabla f^+|^2 H(\phi) + |\nabla f^-|^2 (1 - H(\phi)))dxdy + \nu \int_\Omega |\nabla H(\phi)|.$$

This model can be extended to segment an image with intensity inhomogeneity and include two or more phases.

Figure 2.9 shows an initial noisy image I_0 and initial contours with the evolving curve superimposed. The denoised version f of I_0 is shown on the far right. Clearly, the model performs well with active contours, denoising,

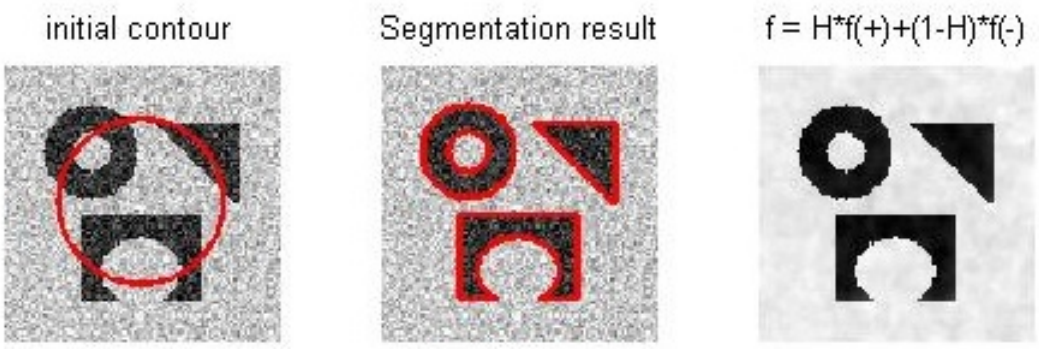

Figure 2.9: Segmentation results of the PS model

and edge-detection, and several objects of distinct intensities are correctly segmented with only one level set function. Even though the PS model can segment an image by reducing the influence of intensity inhomogeneity, it is computationally expensive and inefficient in practice.

Compared to the PS model, a more inexpensive and accurate model was proposed by Li et al. [11, 12]. This model is called local binary fitting (LBF), which applies local intensity information as constraints. The main idea is to introduce two spatially varying fitting functions $f_1(x)$ and $f_2(x)$ to approximate the local intensities inside and outside of the contour, respectively. The local data fitting term is defined as follows in level set formulation:

$$E^{LBF}(\phi, f_1, f_2) = \lambda_1 \int [K_\sigma(x-y)|I_0(y) - f_1(x)|^2 H(\phi(y))dy]dx + \lambda_2 \int [K_\sigma(x-y)|I_0(y) - f_2(x)|^2 (1 - H(\phi(y)))dy]dx. \tag{2.15}$$

where H is the Heaviside function, K_σ is a Gaussian kernel with standard deviation σ, and λ_1 and λ_2 are positive constants; in most cases, $\lambda_1 = \lambda_2 = 1$.

The distance regularizing term $P(\phi)$ in (2.3) is incorporated into the LBF model to give stable evolution of the level set function ϕ. In addition, it is

necessary to smooth the zero level set ϕ by penalizing its length, given by

$$L(\phi) = \int_{\Omega} \delta(\phi(x))|\nabla\phi(x)|dx. \tag{2.16}$$

Thus, the efficient energy can be written as follows:

$$F(\phi, f_1, f_2) = E^{LBF}(\phi, f_1, f_2) + \mu P(\phi) + \nu L(\phi) \tag{2.17}$$

where μ and ν are positive constants. Incorporating the distance regularizing term into the LBF energy functional renders, the re-initialization process unnecessary; thus, the LBF method is computational inexpensive and efficient.

To minimize the energy functional (2.17), the standard gradient descent method is used. Minimizing $F(\phi, f_1, f_2)$ with respect to ϕ for fixed f_1 and f_2, the gradient descent flow is derived as

$$\frac{\partial\phi}{\partial t} = -\delta_\epsilon(\phi)(\lambda_1 e_1 - \lambda_2 e_2) + \nu\delta_\epsilon(\phi)div(\frac{\nabla\phi}{|\nabla\phi|}) + \mu(\nabla^2\phi - div(\frac{\nabla\phi}{|\nabla\phi|})) \tag{2.18}$$

where δ_ϵ is the regularized version of the Dirac delta function, and e_1 and e_2 are given by

$$e_1(x) = \int_{\Omega} K_\sigma(y-x)|I_0(x) - f_1(y)|^2 dy$$

and

$$e_2(x) = \int_{\Omega} K_\sigma(y-x)|I_0(x) - f_2(y)|^2 dy.$$

Here, f_1 and f_2 are defined by minimizing $F(\phi, f_1, f_2)$ for a fixed level set function ϕ. Using calculus of variations, these functions are given by

$$f_1(x) = \frac{K_\sigma(x) * [H_\epsilon(\phi(x))I_0(x)]}{K_\sigma(x) * H_\epsilon(\phi(x))} \tag{2.19}$$

and

$$f_2(x) = \frac{K_\sigma(x) * [(1 - H_\epsilon(\phi(x)))I_0(x)]}{K_\sigma(x) * [1 - H_\epsilon(\phi(x))]} \tag{2.20}$$

where H_ϵ is the regularized version of the Heaviside function.

Note that the standard deviation σ of the kernel plays an important role. It can be viewed as a scale parameter that controls the region-scalability from small neighborhoods to the entire image domain [12]. The scale parameter should be properly chosen according to the contents of a given image. In particular, when an image is too noisy or has low contrast, a large value of σ should be chosen. Unfortunately, this may cause a high computational cost. Small values of σ can cause undesirable result as well. Because of f_1 and f_2 in (2.19),(2.20), the LBF model is able to handle images with intensity inhomogeneity. These functions can be viewed as the weighted averages of the image intensities in a Gaussian window inside and outside the contour, respectively.

Inspired by the LBF model [11], a more computationally efficient and accurate model was proposed by Zhang et al. [14]. They defined the local fitted image as

$$I^{LFI} = m_1 H(\phi) + m_2(1 - H(\phi)) \tag{2.21}$$

where

$$\begin{cases} m_1 = \text{mean}(I_0 \in (\{x \in \Omega | \phi(x) < 0\} \cap W_k(x))) \\ m_2 = \text{mean}(I_0 \in (\{x \in \Omega | \phi(x) > 0\} \cap W_k(x))). \end{cases} \tag{2.22}$$

The rectangular window function is denoted by $W_k(x)$. A Gaussian kernel is used to regularize the level set function instead of the traditional regularizing term $div(\nabla\phi/|\nabla\phi|)\delta(\phi)$ as mentioned in Section 2.1.

Then proposed local intensity fitting (LIF) energy formulation is given by

$$E^{LIF} = \frac{1}{2}\int_{\Omega} |I_0(x) - I^{LFI}(x)|^2 dx \ , \quad x \in \Omega \tag{2.23}$$

where, I^{LFI} is a local fitted image, which defined in (2.21).

In this model, a Gaussian filtering is applied to regularize the level set function, i.e., $\phi = G_\gamma * \phi$, where γ is the standard deviation. This method can segment an images with intensity inhomogeneity or multiple objects with different intensities.

The local and global intensity fitting (LGIF) method [13] takes advantage of the Chan-Vese and LBF models by combining local and global intensity information to handle intensity inhomogeneity. The local intensity fitting energy E^{LIF} is equal to the LBF model, and the global intensity fitting (GIF) energy E^{GIF} is the fitting term of the Chan-Vese model:

$$E^{GIF}(\phi, c_1, c_2) = \int |I_0(x) - c_1|^2 H(\phi(x))dx + \int |I_0(x) - c_2|^2 (1 - H(\phi(x)))dx.$$

The LGIF method defined the energy functional as follows:

$$\begin{aligned} E^{LGIF}(\phi, c_1, c_2, f_1, f_2) = (1-\omega)E^{LIF}(\phi, f_1, f_2) + \omega E^{GIF}(\phi, c_1, c_2) \\ + \nu L(\phi) + \mu P(\phi) \end{aligned} \tag{2.24}$$

where f_1 and f_2 are the optimal fitting functions given by (2.19) and (2.20), $L(\phi)$ is length of the zero level set for smoothing given by (2.16), $P(\phi)$ is the deviation of the level set function from the signed distance function in (2.3) to eliminate re-initialization process, and ω is a positive constant such that ($0 \leq \omega \leq 1$). The value of ω should be small when the intensity inhomogeneity in an image is severe.

2.4 Shape prior segmentation models

The previous methods fail to segment images with missing or misleading information due to noise, occlusion, or low-contrast. Therefore, shape prior knowledge is incorporated to improve the robustness of these segmentation methods. Method based on shape's level set knowledge were first introduced by Chen et al. [25, 26]. They modified the Geodesic Active Contour model by adding a shape term. Their model is able to find boundaries that are similar to the shape prior, even when the boundary has gaps in the image.

Level set representation of the shape prior was introduced in [32, 33]. Let $\phi : \Omega \to R^2$ be a Lipchitz function that refers to the level set representation of a given shape S. This shape defines a region R in the image domain Ω. The shape representation is defined by

$$\phi_S(x,y) = \begin{cases} 0 & \text{if } (x,y) \in S \\ +D((x,y),S) > 0, & \text{if } (x,y) \in R_S \\ -D((x,y),S) < 0, & \text{if } (x,y) \in \Omega \setminus R_S \end{cases} \tag{2.25}$$

where $D((x,y),S)$ is the minimum Euclidean distance between the grid location (x,y) and shape S. Level set knowledge-based models represent a shape according to (2.25).

Many models focus only on segmenting the desired objects. Cremers et al.'s model, however, can also segment other objects by introducing a labeling function [9]. This model is given by

$$E^{Cremers}(c_1,c_2,\phi,L) = E^{Chan-Vese}(c_1,c_2,\phi) + E_{shape}(\phi,L). \tag{2.26}$$

The shape term $E_{shape}(\phi,L)$ has three options: E^{global}_{shape},E^{static}_{shape}, and $E^{dynamic}_{shape}$. The global shape prior is formulated as

$$E^{global}_{shape}(\phi) = \alpha \int_\Omega (\phi(x) - \phi_0(x))^2 dx \tag{2.27}$$

where ϕ_0 is the level set function embedding a given shape prior, and α controls the weight of the prior shape. The global shape term of Cremers et

al.'s has the ability to ignore objects that do not require segmentation. Static energy segments all objects in an image. The static shape term is given by

$$E_{shape}^{static}(\phi, L) = \alpha \int_{\Omega} (\phi(x) - \phi_0(x))^2 (L+1)^2 dx \tag{2.28}$$

where L is a static labeling function used to indicate the region where the shape prior should be active. Labeling function L is either $+1$ and -1 depending on whether the prior should be enforced or not. Note that, the labeling function must be specified beforehand.

By minimizing the total energy with dynamic shape term with respect to L and ϕ, prior knowledge of the labeling function can be avioded. The dynamic shape term is given by

$$\begin{aligned} E_{shape}^{dynamic}(\phi, L) = \alpha \int_{\Omega} (\phi(x) - \phi_0(x))^2 (L+1)^2 dx \\ + \int_{\Omega} \lambda^2 (L-1)^2 dx + \gamma \int_{\Omega} |\nabla H(L)| dx. \end{aligned} \tag{2.29}$$

Compared to the static labeling function, this labeling function is dynamic, i.e., it does not need to be specified beforehand. It can control the region where the shape prior is enforced and the smoothness of the boundary separating the regions. If the labeling function is not included in the shape term of Cremers et al.'s model, the other objects in a given image are not segmented as shown in Fig.(2.10). In contrast, by incorporating the labeling function, the other objects are segmented as shown in Fig.(2.11).

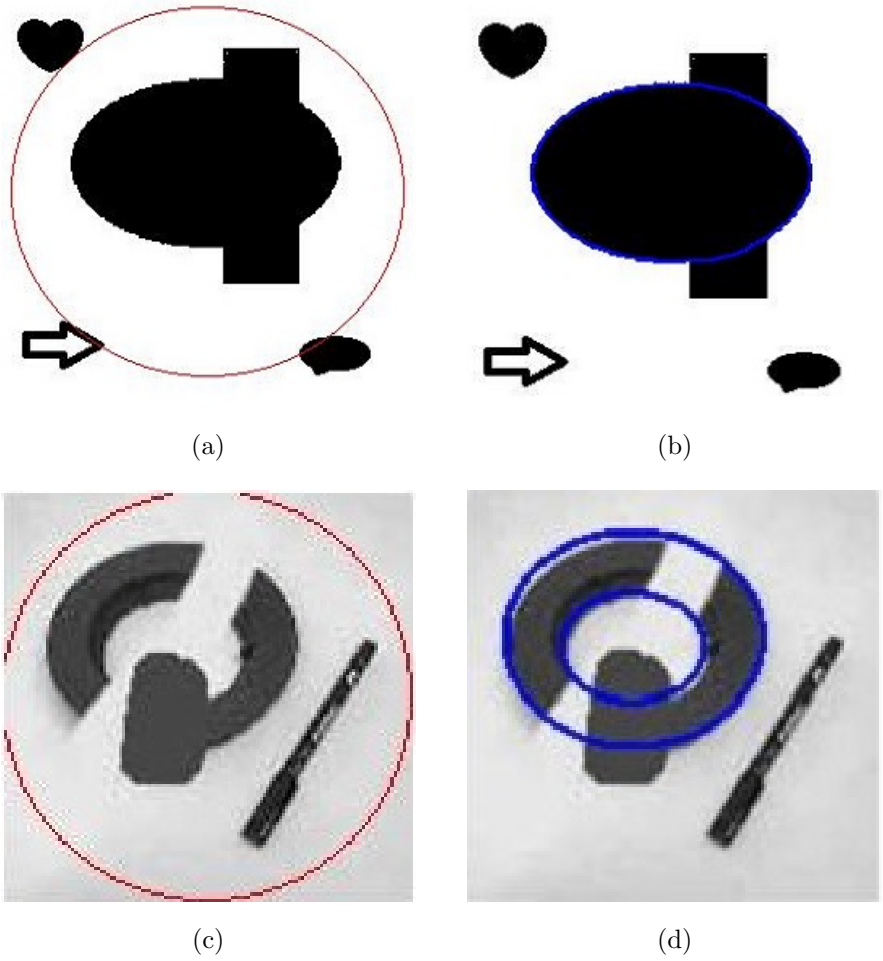

(a) (b)

(c) (d)

Figure 2.10: Results of Cremers et al.'s model: initial level sets are shown in (a) and (c), and segmentation results without the labeling function are shown in (b) and (d).

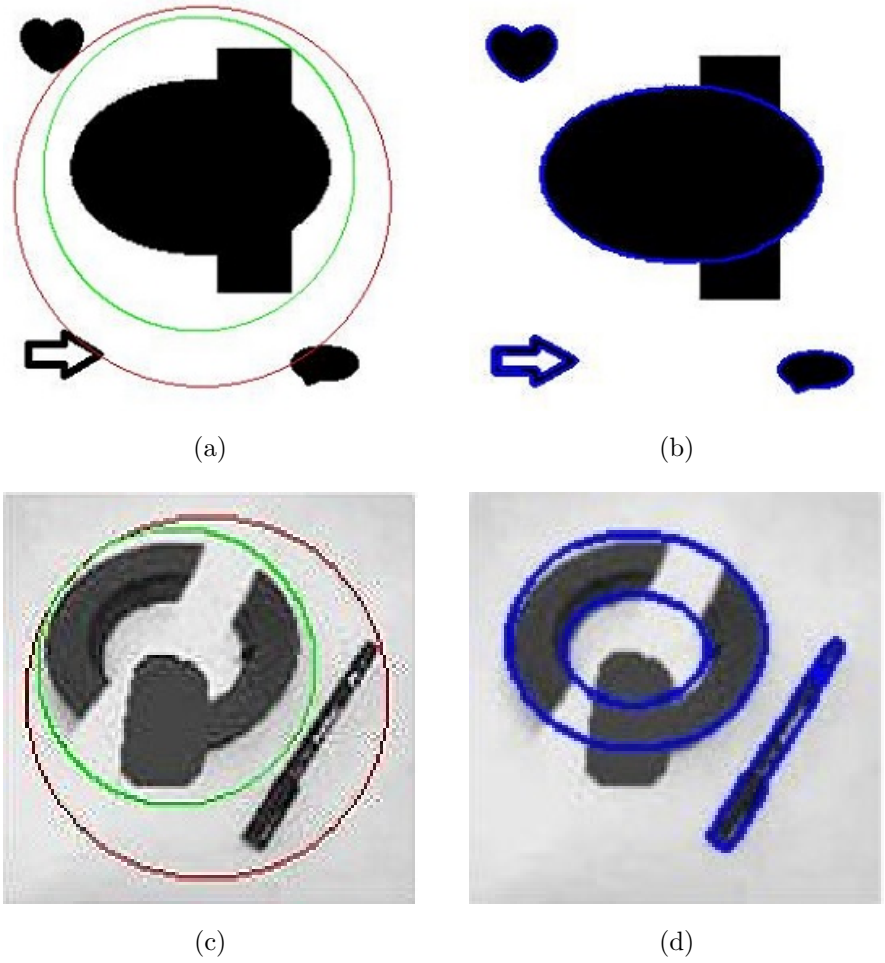

(a) (b)

(c) (d)

Figure 2.11: Results of Cremers et al.'s model: initial level sets are shown in (a) and (c), and segmentation results with the labeling function are shown in (b) and (d).

Cremers et al.'s model can be extended to multiple-region images as well [42]:

$$\begin{aligned}
E_{extension}^{Cremers} &= \int_{\Omega}((I_0 - c_{11})^2 H(\phi_1)H(\phi_2) + (I_0 - c_{10})^2 H(\phi_1)(1 - H(\phi_2)))dx \\
&+ \int_{\Omega}((I_0 - c_{01})^2 (1 - H(\phi_1))H(\phi_2) + (I_0 - c_{00})^2 (1 - H(\phi_1))(1 - H(\phi_2)))dx \\
&+ \nu_1 \int_{\Omega} |\nabla H(\phi_1)|dx + \nu_2 \int_{\Omega} |\nabla H(\phi_2)|dx \\
&+ \alpha_1 \int_{\Omega} (\phi_1(x) - \phi_{shape1}(x))^2 (L_1 + 1)^2 dx \\
&+ \alpha_2 \int_{\Omega} (\phi_2(x) - \phi_{shape2}(x))^2 (L_2 + 1)^2 dx
\end{aligned}$$

where c_{11}, c_{01}, c_{10} and c_{00} are the mean intensities in each region given by

$$\begin{aligned}
c_{11} &= mean(I) \text{ in}\{x : \phi_1 > 0, \phi_2 > 0\} \\
c_{01} &= mean(I) \text{ in}\{x : \phi_1 > 0, \phi_2 < 0\} \\
c_{10} &= mean(I) \text{ in}\{x : \phi_1 < 0, \phi_2 > 0\} \\
c_{00} &= mean(I) \text{ in}\{x : \phi_1 < 0, \phi_2 < 0\}.
\end{aligned}$$

Figure 2.12 shows the results of the extended model. Two level set functions ϕ_1 and ϕ_2 are used to segment objects with shape priors. In the presence of labeling functions L_1 and L_2, the other objects are also segmented.

No transformation is allowed for the prior shape in Cremers et al.'s model, whereas the prior shape is geometrically transformed in the Chan-Zhu model [9]. The concepts of invariance to translation, rotation and scaling are defined for a set of objects.

Definition 2.4.1. Any two objects are said to be equivalent if they have the same shape.

In other words, their signed distance functions are related. Let ψ and ψ_0 be the signed distance functions of two objects S_1 and S_2, of the same shape. Then, there exists a four-tuple (a, b, r, θ) such that:

$$\psi(x, y) = r\psi_0(x^*, y^*) \tag{2.30}$$

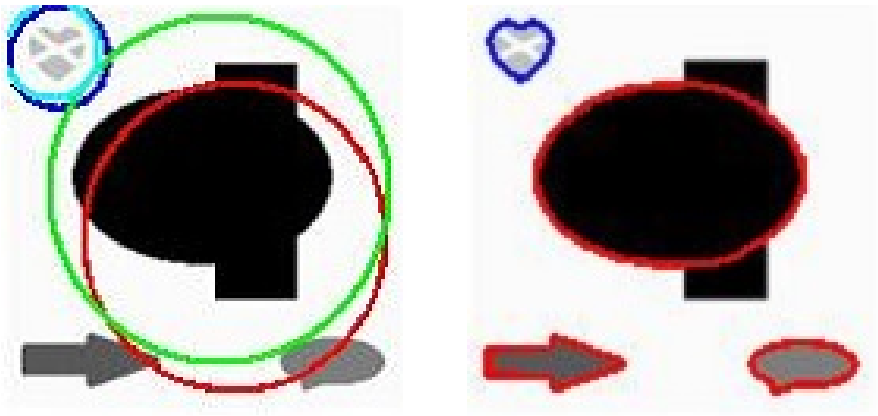

(a) (b)

Figure 2.12: Segmentation results of shapes:(a)Initial ϕ_1 (blue) for an occluded object and ϕ_2 (red) for an object with missing information. Labeling functions L_1 and L_2- are sky blue and green, respectively, (b) segmentation results

where

$$\begin{cases} x^* = \frac{(x-a)\cos(\theta)+(y-b)\sin(\theta)}{r} \\ y^* = \frac{-(x-a)\sin(\theta)+(y-b)\cos(\theta)}{r} \end{cases}$$

and (a, b), r and θ represent the translation, scaling and rotation parameters, respectively. The proposed simple shape energy is given by

$$E_{shape}^{simple}(\phi, \psi) = \int_{\Omega} (H(\phi) - H(\psi))^2 dx \tag{2.31}$$

where ϕ is a level set function for segmentation, ψ_0 is the signed distance function of a given prior shape, and ψ is the fixed signed distance function in (2.30) of the shape. Therefore, the total energy of the Chan-Zhu model is

$$E^{Chan-Zhu}(\phi, \psi, c_1, c_2) = E^{Chan-Vese}(\phi, c_1, c_2) + \lambda E_{\text{shape}}^{simple}(\phi, \psi). \tag{2.32}$$

More explicitly,

$$E(c_1, c_2, \phi, \psi) = \int_\Omega ((I_0 - c_1)^2 H(\phi) + (I_0 - c_2)^2 (1 - H(\phi)))dx + \mu \int_\Omega |\nabla H(\phi)| + \lambda \int_\Omega (H(\phi) - H(\psi))^2 dx. \tag{2.33}$$

Chan and Zhu extended their model by introducing labeling function L. In general case, the shape term is

$$E_{shape}^{general}(\phi, \psi, L) = \int_\Omega (H(\phi)H(L) - H(\psi))^2 dx + \mu_1 \int_\Omega (1 - H(L))dx + \mu_2 \int_\Omega |\nabla H(L)|dx \tag{2.34}$$

where $H(\phi)H(L)$ characterizes the intersection of $\phi > 0$ and $L > 0$. The second term in (2.34) encourages the area in region $\{(x, y) \in \Omega : L(x, y) > 0\}$, and the last term smooths the boundary separated by L in domain Ω.

In Fig.2.13(a), the initial level set ϕ_0 is represented by a green circle, and the prior shape ψ of a hand is shown in blue. Although the Chan-Zhu model allows geometric transformations of the shape prior, it can only segment an object with shape prior information (see Fig.2.13(c)).

(a) (b) (c)

Figure 2.13: Results of the Chan-Zhu model:(a) initial (green) and prior shape (blue), (b) segmentation results for ϕ, and (c) segmentation results for ψ.

Alternatives to the generalized Chan-Zhu model are developed in [27, 28]. Thiruvenkadam et al. considered selective shape priors to segment multiple

occluded objects. Their proposed energy can be written as

$$\begin{aligned} E(\Phi, C, T) = \sum_{i=1}^{4} \int_{\Omega} (I_0 - c_i m_i)^2 dx + \lambda \Big(\int_{\Omega} |\nabla H(\phi_1)| + \int_{\Omega} |\nabla H(\phi_2)| \Big) \\ + \int_{\Omega} \{\beta + \beta_1 H(\phi_2)(c_3 - c_2)^2\} (H(\phi_1) - S \circ T_1)^2 dx \\ + \int_{\Omega} \{\beta + \beta_1 H(\phi_1)(c_3 - c_1)^2\} (H(\phi_2) - S \circ T_2)^2 dx \end{aligned} \tag{2.35}$$

where $m_1 = H(\phi_1)$, $m_2 = H(\phi_2)$, $m_3 = H(\phi_1)H(\phi_2)$, and $m_4 = (1 - H(\phi_1))(1 - H(\phi_2))$. Two level set functions ϕ_1 and ϕ_2 are used to define the following four regions: $\{\phi_1 > 0\}$, $\{\phi_2 > 0\}$, $\{\phi_1 > 0,\ \phi_2 > 0\}$ and $\{\phi_1 < 0,\ \phi_2 < 0\}$, and, where c_1, c_2, c_3 and c_4 are mean intensities in each region, respectively. Function S embeds one shape prior, and $T_k = [\mu_k, \theta_k, \mathbf{t}_k]$ are rigid transformations with scale factor μ_k, rotation factor θ_k and translation factor $\mathbf{t}_k$ for $k = 1, 2$.

Chapter 3

Proposed models

3.1 Global and local image fitting energy

Inspired by Wang et al.'s model, we take advantages of the LIF model and the Chan-Vese model, to reduce the computational complexity and cost, and to improve the convergence speed by eliminating the segmentation process' sensitivity to initialization. First, we recall the LIF model and the Chan-Vese models. The LIF model is given by:

$$E^{LIF}(\phi) = \frac{1}{2}\int_{\Omega} |I_0(x) - m_1 H(\phi(x)) - m_2(1 - H(\phi(x)))|^2 dx \tag{3.1}$$

where

$$\begin{cases} m_1 = \text{mean}(I_0 \in (\{x \in \Omega | \phi(x) < 0\} \cap K_\sigma(x))) \\ m_2 = \text{mean}(I_0 \in (\{x \in \Omega | \phi(x) > 0\} \cap K_\sigma(x))). \end{cases}$$

Equation (3.1) uses a Gaussian kernel to regularize the level set function ϕ, i.e., $\phi = G_\xi * \phi$.

The Chan-Vese model is given by:

$$\begin{aligned} E^{Chan-Vese}(c_1, c_2, \phi) = &\int_{\Omega} ((I_0 - c_1)^2 H(\phi) + (I_0 - c_2)^2 (1 - H(\phi)))dx \\ &+ \mu \int_{\Omega} |\nabla H(\phi)| dx + \nu \int_{\Omega} H(\phi) dx. \end{aligned} \tag{3.2}$$

The fitting term of the Chan-Vese model, excluding regularization terms, is given by:

$$E^{GIF} = \int_{\Omega} (|I_0 - c_1|^2 H(\phi) + |I_0 - c_2|^2 (1 - H(\phi)))dx. \tag{3.3}$$

We call this term by global image fitting (GIF) term.

The proposed energy functional consists of a local image fitting term and global image fitting term. Specifically,

$$E^{M.LIF} = E^{LIF} + \alpha E^{GIF} \tag{3.4}$$

where α is a positive constant such that $(0 \leq \alpha \leq 1)$. The value of α should be small for images with severe intensity inhomogeneity.

The local image fitting term includes a local force to attract the contours and stop it at object boundaries. This enables the model to cope with intensity inhomogeneity. The global image fitting term includes a global force to drive the motion of the contour far away from object boundaries. This allows flexible initialization of the contours. The modified LIF energy can be written as

$$\begin{aligned} E^{M.LIF}(\phi, c_1, c_2) = \frac{1}{2} \int_{\Omega} |I_0(x) - m_1 H(\phi) - m_2(1 - H(\phi))|^2 dx \\ + \alpha \int_{\Omega} (|I_0 - c_1|^2 H(\phi) + |I_0 - c_2|^2 (1 - H(\phi)))dx. \end{aligned} \tag{3.5}$$

Expressing m_1 and m_2 using the level set function ϕ yeilds

$$\begin{cases} m_1 & = \frac{K_\sigma * (H(\phi) I_0(x))}{K_\sigma * (H(\phi))} \\ m_2 & = \frac{K_\sigma * ((1 - H(\phi)) I_0(x)))}{K_\sigma * (1 - H(\phi))}. \end{cases}$$

The influence of the local and global forces on the curve evolution is complementary. The local force is dominant near the object boundaries, while the global force is dominant at locations far away from object boundaries.

The standard deviation σ of the kernel and regularizing parameter γ play an important role. Standard deviation σ is a scale parameter that controls

the region-scalability from small neighborhoods to the entire image domain. The scale parameter should be properly chosen depending on the contents of an image. In particular, when image is noisy or has low contrast, σ should be large. Unfortunately, this results in a high computational cost. In the same way, values of σ that are too small produce undesirable side effects as well. In general, γ should be chosen between 0.5 and 1.

We now discuss the numerical approximation for minimizing the $E^{M.LIF}$ functional. Constants c_1 and c_2 that minimize the energy in (3.5) are given by

$$c_1 = \frac{\int I_0(x)H(\phi(x))dx}{\int H(\phi(x))dx}, c_2 = \frac{\int I_0(x)(1-H(\phi(x)))dx}{\int(1-H(\phi(x)))dx} \tag{3.6}$$

Calculus of variations [39] allows us to add variation ζ to the level set function ϕ such that $\bar{\phi} = \phi + \epsilon\zeta$. For fixed c_1 and c_2, differentiating with respect to ϕ, and letting $\epsilon \to 0$ produces

$$\begin{aligned}
\frac{\delta E^{M.LIF}}{\delta\phi} &= \lim_{\epsilon\to 0}\frac{d}{d\epsilon}(\frac{1}{2}\int_\Omega |I_0(x) - m_1H_\epsilon(\bar{\phi}) - m_2(1-H_\epsilon(\bar{\phi}))|^2dx \\
&+ \alpha\int_\Omega(|I_0-c_1|^2H_\epsilon(\bar{\phi}) + |I_0-c_2|^2(1-H_\epsilon(\bar{\phi})))dx) \\
&= \lim_{\epsilon\to 0}(-\int_\Omega \delta_\epsilon(\bar{\phi})\{I_0 - m_1H_\epsilon(\bar{\phi}) - m_2(1-H_\epsilon(\bar{\phi}))\}(m_1-m_2)\zeta dx \\
&+ \alpha\int_\Omega \delta_\epsilon(\bar{\phi})(-(I_0-c_1)^2 + (I_0-c_2)^2)\zeta dx) \\
&= -(\int_\Omega \delta_\epsilon(\phi)\{I_0 - m_1H_\epsilon(\phi) - m_2(1-H_\epsilon(\phi))\}(m_1-m_2)\zeta dx \\
&+ \alpha\int_\Omega \delta_\epsilon(\phi)(-(I_0-c_1)^2 + (I_0-c_2)^2)\zeta dx).
\end{aligned}$$

Therefore we obtain the Euler-Lagrange equation

$$\delta_\epsilon(\phi)\{(I_0 - I^{LFI})(m_1-m_2) + \alpha(-(I_0-c_1)^2 + (I_0-c_2)^2)\} = 0$$

where $I^{LFI} = m_1H_\epsilon(\phi) + m_2(1-H_\epsilon(\phi))$. The regularized versions of the

Heaviside and Dirac delta functions are

$$\begin{aligned} H_\epsilon(\phi) &= \frac{1}{2}(1 + \frac{2}{\pi}\arctan(\frac{\phi}{\epsilon})) \\ \delta_\epsilon(\phi) &= \frac{1}{\pi} \cdot \frac{\epsilon}{\epsilon^2 + \phi^2}. \end{aligned} \tag{3.7}$$

Using the steepest gradient descent method, we obtain the following gradient descent flow

$$\frac{\partial \phi}{\partial t} = \delta_\epsilon(\phi)\{(I_0 - I^{LFI})(m_1 - m_2) + \alpha(-(I_0 - c_1)^2 + (I_0 - c_2)^2)\}. \tag{3.8}$$

The algorithm for solving $E^{M.LIF}$ is as follows:

Step 1: Initialize the level set function ϕ.

Step 2: Compute c_1 and c_2 according to (3.6).

Step 3: Evolve the level set function ϕ according to (3.8).

Step 4: Regularize the level set function ϕ using a Gaussian kernel, i.e., $\phi = G_\gamma * \phi$, where γ is the standard deviation.

Step 5: Check whether the evolution is stationary. If not, return to step 3.

Using gradient descent flow (3.8) and the above algorithm, segmentation results are produced faster and require fewer iteration than the LBF, LGIF and LIF models. Experimental results are illustrated in Fig.3.1. Our algorithm works well on images with intensity inhomogeneity and segmenting multiple objects with different intensities (Figs.3.1(b),(e) and (h)). The scale parameter σ is equal to 3 for these images and the regularizing parameter γ is properly chosen between 0.65 and 0.85. These results are similar to the results of the LIF, LBF, and LGIF models.

The proposed model allows flexible initialization of contours as shown in Fig.3.2. We tested our method using other initial contours (see Figs.3.2(a),(d) and (g)) and the same parameters as in Fig.3.1. As seen Figs.3.2(c),(f) and (i), the LIF model does not work well for these initial conditions. We also tested the LGIF method using different initial contours as shown in Figs.3.2(a),(d) and (g). Notice that same results are produced by our method. Computational times are relatively high using the LGIF method, however. In Table1, we compare the number of iterations and computational times for the LBF, LGIF, LIF models to our proposed method.

Table 3.1: Computation time results.

Methods	Vessel(a)	Vessel (c)	Synthetic one (e)
	Iterations(time(s))	Iterations(time(s))	Iterations(time(s))
LBF	300 (2.41)	280 (2.03)	900 (9.82)
LGIF	220 (2.05)	150 (1.29)	800 (8.47)
LIF	200 (1.16)	200 (0.94)	600 (4.43)
M.LIF	120 (0.49)	100 (0.41)	400 (1.97)

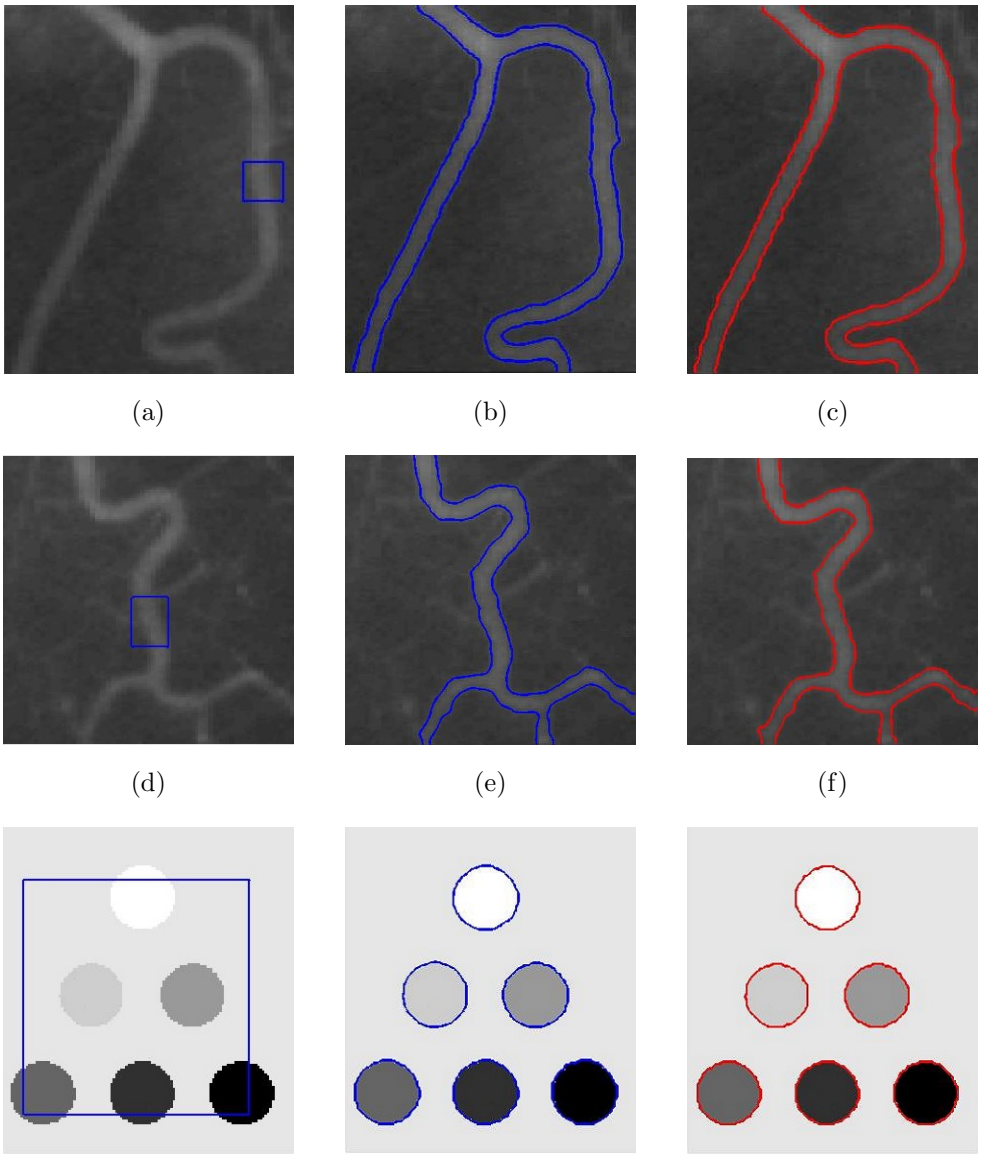

Figure 3.1: Segmentation results of the modified LIF method: (a), (d) and (g) are the given images with the initial level set; (b), (e) and (h) are the results of the modified LIF model; (c), (f) and (i) are the results of the LGIF model.

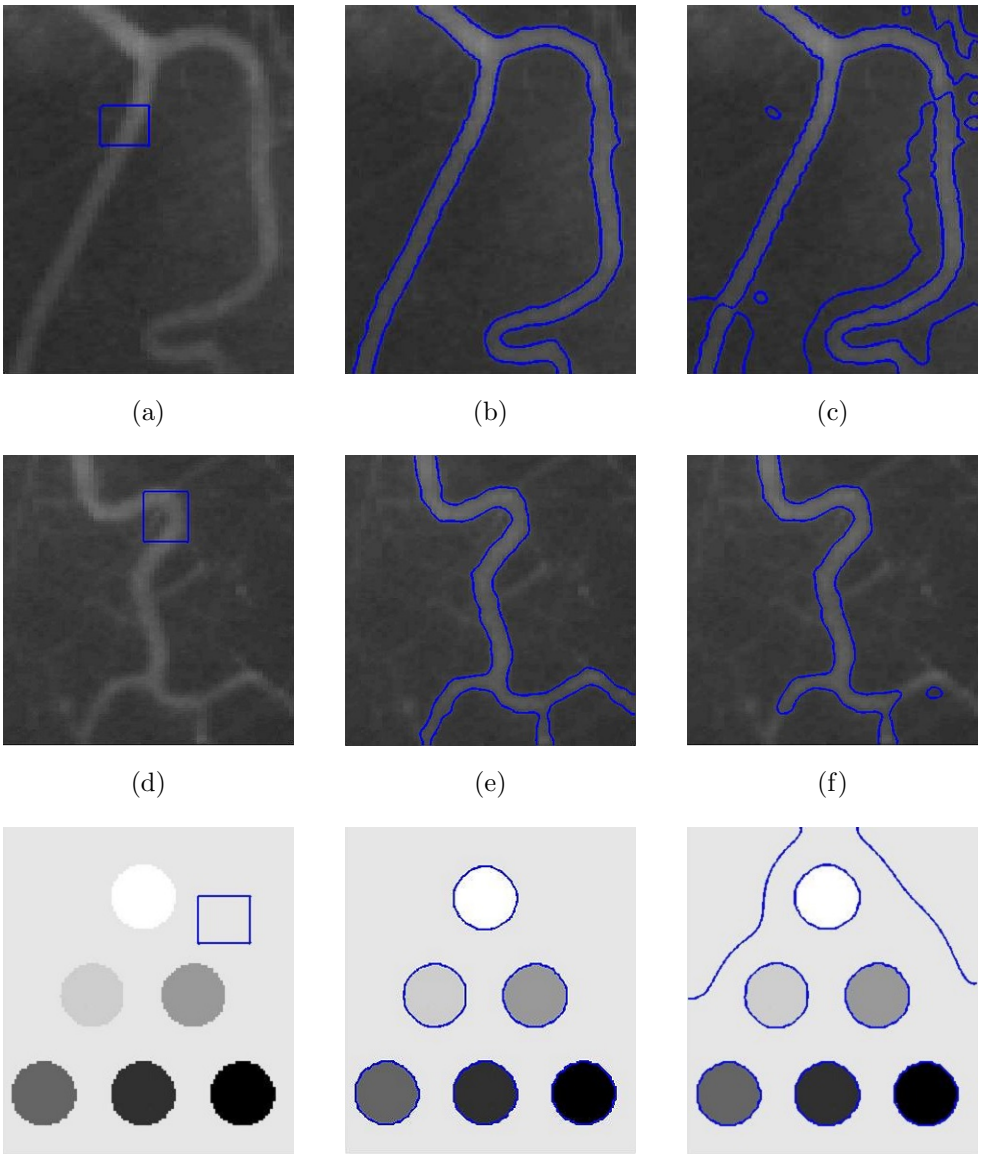

Figure 3.2: Segmentation results of the modified LIF method: (a), (d) and (g) are the given images with the initial level set; (b), (e) and (h) the results of the modified LIF model; (c), (f) and (i) are the results of the LIF model.

3.2 Global and local image fitting energy with shape prior

Simpler active contour methods fail to segment images with missing or misleading information due to noise, occlusion, or low-contrast. Therefore, shape prior knowledge is incorporated to improve the robustness of such segmentation methods. Fundamental methods for shape prior segmentation have a general energy functional that is a linear combination of segmentation energy and shape energy. Analogous to the general energy functional, we propose a method that can be viewed as minimizing the total energy of our modified LIF energy and the shape energy.

Our method consider two cases. In the first case, the prior shapes are located exactly at the placement of the desired objects and have the same scales and pose as the desired objects; thus, no transformations is required. Let ψ_0 be the signed distance function of the prior shape and L be a static labeling function. The labeling function takes on the values $+1$ and -1 depending on whether the prior shape is enforced or not.

The formulation of our energy is as follows:

$$E(\phi, \psi_0) = E^{M.LIF} + \beta \int_\Omega (H(\phi) - H(\psi_0))^2 (L+1)^2 dx \tag{3.9}$$

where $H(\cdot)$ is the Heaviside function and $E^{M.LIF}$ is our modified LIF model described in Section 3.1. More explicitly,

$$\begin{aligned} E(\phi, \psi_0, c_1, c_2) = \frac{1}{2} \int_\Omega |I_0(x) - m_1 H(\phi) - m_2(1 - H(\phi))|^2 dx \\ + \alpha \int_\Omega (|I_0 - c_1|^2 H(\phi) + |I_0 - c_2|^2 (1 - H(\phi))) dx \\ + \beta \int_\Omega (H(\phi) - H(\psi_0))^2 (L+1)^2 dx. \end{aligned} \tag{3.10}$$

Numerical approximations of this model are discussed in previous sections. Calculus of variation allows us to add variation ζ to the level set function ϕ

such that $\bar{\phi} = \phi + \epsilon\zeta$. Fixing c_1 and c_2, differentiating with respect to ϕ, and letting $\epsilon \to 0$ yeilds

$$\begin{aligned}
\frac{\delta E(\phi, \psi_0)}{\delta \phi} &= \lim_{\epsilon \to 0} \frac{d}{d\epsilon}(\frac{1}{2}\int_\Omega |I_0(x) - m_1 H_\epsilon(\bar{\phi}) - m_2(1 - H_\epsilon(\bar{\phi}))|^2 dx \\
&+ \alpha \int_\Omega (|I_0 - c_1|^2 H_\epsilon(\bar{\phi}) + |I_0 - c_2|^2(1 - H_\epsilon(\bar{\phi})))dx \\
&+ \beta \int_\Omega (H_\epsilon(\bar{\phi}) - H_\epsilon(\psi_0))^2 (L+1)^2 dx) \\
&= \lim_{\epsilon \to 0}(-\int_\Omega \delta_\epsilon(\bar{\phi})\{I_0 - m_1 H_\epsilon(\bar{\phi}) - m_2(1 - H_\epsilon(\bar{\phi}))\}(m_1 - m_2)\zeta dx \\
&+ \alpha \int_\Omega \delta_\epsilon(\bar{\phi})(-(I_0 - c_1)^2 + (I_0 - c_2)^2)\zeta dx \\
&- 2\beta \int_\Omega \delta_\epsilon(\bar{\phi})(H_\epsilon(\bar{\phi}) - H_\epsilon(\psi_0))(L+1)^2 \zeta dx) \\
&= -(\int_\Omega \delta_\epsilon(\phi)\{I_0 - m_1 H_\epsilon(\phi) - m_2(1 - H_\epsilon(\phi))\}(m_1 - m_2)\zeta dx \\
&+ \alpha \int_\Omega \delta_\epsilon(\phi)(-(I_0 - c_1)^2 + (I_0 - c_2)^2)\zeta dx \\
&- 2\beta \int_\Omega \delta_\epsilon(\phi)(H_\epsilon(\phi) - H_\epsilon(\psi_0))(L+1)^2 \zeta dx).
\end{aligned}$$

Therefore, using the steepest descent method, we obtain the Euler-Lagrange equation

$$\begin{aligned}
\delta_\epsilon(\phi)\{(I_0 - I^{LFI})(m_1 - m_2) + \alpha(-(I_0 - c_1)^2 + (I_0 - c_2)^2) \\
- 2\beta(H_\epsilon(\phi) - H_\epsilon(\psi_0))(L+1)^2\} = 0.
\end{aligned}$$

The gradient descent flow of energy (3.10) is given by:

$$\begin{aligned}
\frac{\partial \phi}{\partial t} &= \delta_\epsilon(\phi)\{(I_0 - I^{LFI})(m_1 - m_2) + \alpha(-(I_0 - c_1)^2 + (I_0 - c_2)^2)\} \\
&- 2\beta\delta_\epsilon(\phi)(H_\epsilon(\phi) - H_\epsilon(\psi_0))(L+1)^2.
\end{aligned} \tag{3.11}$$

If we minimize the above energy with respect to c_1 and c_2 for fixed ϕ, the optimal values of c_1 and c_2 are obtained using (3.6).

The algorithm for solving $E(\phi, \psi_0)$ is given in Table 3.2.

Table 3.2: Method for solving $E(\phi, \psi_0)$.

A) **Definitions**:

I_0 : Initial image to segment

Ω : Image domain

ψ_0 : Given shape

ϕ : Level set function for segmentation

L : Labeling function

β : Parameter weight of the shape term

$\delta_\epsilon(\phi)$: Regularized Dirac-delta function of ϕ defined by (3.7)

$H_\epsilon(\phi)$: Regularized Heaviside function of ϕ defined by (3.7)

G_γ : Gaussian filtering with standard deviation γ

t : Step size

α : Parameter for intensity inhomogeneity

B) **Set initial conditions**:

Initialize ϕ at $t = 0$ as $\phi(x, t = 0) = \begin{cases} \omega & \text{if } x \in \Omega \setminus \Omega_0 \\ 0 & \text{if } x \in \partial\Omega_0 \\ -\omega & \text{if } x \in \Omega_0 \setminus \partial\Omega_0 \end{cases}$

where $\omega > 0$ is a constant, Ω_0 is a subset of Ω and
$\partial\Omega_0$ is the boundary of Ω_0.
Labeling function L is set to either $+1$ and -1 depending on
whether the prior shape is enforced or not

C) **For** $n : n = 1, 2, \ldots$

1) Compute c_1 and c_2 using (3.6)

2) Evolve the level set function ϕ according to (3.11).

3) Regularize the level set function ϕ using the Gaussian kernel,
i.e., $\phi = G_\gamma * \phi$, where γ is the standard deviation.

4) Check whether the evolution is stationary. If not, return to Step 2.

For the second case of our model, the prior shape ψ_0 is placed at arbitrary locations. The prior shape is transformed to the location, pose, and size according to

$$\begin{cases} x^* = \frac{(x-a-a_{cx})\cos(\theta)+(y-b-b_{cy})\sin(\theta)}{r} + a_{cx} \\ y^* = \frac{-(x-a-a_{cx})\sin(\theta)+(y-b-b_{cy})\cos(\theta)}{r} + b_{cy}. \end{cases} \tag{3.12}$$

The new signed distance function ψ is defined as $\psi(x,y) = r\psi_0(x^*, y^*)$. Then proposed energy is written as

$$E(\phi,\psi) = E^{M.LIF} + \beta \int_\Omega (H(\phi) - H(\psi))^2 (L+1)^2 dx. \tag{3.13}$$

Numerical approximations of minimizing the functional $E(\phi,\psi)$ are performed using the same computation as other proposed models. By theory of calculus of variations, we add variation ζ to the level set function ϕ such that $\bar{\phi} = \phi + \epsilon\zeta$. For fixed c_1 and c_2, differentiating with respect to ϕ, and letting $\epsilon \to 0$ yeilds

$$\begin{aligned} \frac{\delta E(\phi,\psi)}{\delta\phi} &= \lim_{\epsilon\to 0} \frac{d}{d\epsilon}\Big(\frac{1}{2}\int_\Omega |I_0(x) - m_1 H_\epsilon(\bar{\phi}) - m_2(1 - H_\epsilon(\bar{\phi}))|^2 dx \\ &\quad + \alpha \int_\Omega (|I_0 - c_1|^2 H_\epsilon(\bar{\phi}) + |I_0 - c_2|^2 (1 - H_\epsilon(\bar{\phi})))dx \\ &\quad + \beta \int_\Omega (H_\epsilon(\bar{\phi}) - H_\epsilon(\psi))^2 (L+1)^2 dx\Big) \\ &= \lim_{\epsilon\to 0}\Big(-\int_\Omega \delta_\epsilon(\bar{\phi})\{I_0 - m_1 H_\epsilon(\bar{\phi}) - m_2(1 - H_\epsilon(\bar{\phi}))\}(m_1 - m_2)\zeta dx \\ &\quad + \alpha \int_\Omega \delta_\epsilon(\bar{\phi})(-(I_0 - c_1)^2 + (I_0 - c_2)^2)\zeta dx \\ &\quad - 2\beta \int_\Omega \delta_\epsilon(\bar{\phi})(H_\epsilon(\bar{\phi}) - H_\epsilon(\psi))(L+1)^2 \zeta dx\Big) \\ &= -\Big(\int_\Omega \delta_\epsilon(\phi)\{I_0 - m_1 H_\epsilon(\phi) - m_2(1 - H_\epsilon(\phi))\}(m_1 - m_2)\zeta dx \\ &\quad + \alpha \int_\Omega \delta_\epsilon(\phi)(-(I_0 - c_1)^2 + (I_0 - c_2)^2)\zeta dx \\ &\quad - 2\beta \int_\Omega \delta_\epsilon(\phi)(H_\epsilon(\phi) - H_\epsilon(\psi))(L+1)^2 \zeta dx\Big). \end{aligned}$$

Minimizing energy (3.13) with respect to ϕ for fixed c_1 and c_2, results in the following gradient descent flow:

$$\begin{aligned}\frac{\partial \phi}{\partial t} &= \delta_\epsilon(\phi)\{(I_0 - I^{LFI})(m_1 - m_2) + \alpha(-(I_0 - c_1)^2 + (I_0 - c_2)^2)\} \\ &\quad - 2\beta\delta_\epsilon(\phi)(H_\epsilon(\phi) - H_\epsilon(\psi))(L+1)^2.\end{aligned} \tag{3.14}$$

For ψ, note that

$$S(\phi, \psi) = (H_\epsilon(\phi) - H_\epsilon(\psi))(L+1)^2.$$

Thus, the optimal pose parameters are updated according to

$$\frac{\partial a}{\partial t} = \int_\Omega S(\phi, \psi)\{\psi_{0x}(x^*, y^*)\cos(\theta) - \psi_{0y}(x^*, y^*)\sin(\theta)\}\delta_\epsilon(\psi)dxdy \tag{3.15}$$

$$\frac{\partial b}{\partial t} = \int_\Omega S(\phi, \psi)\{\psi_{0x}(x^*, y^*)\sin(\theta) + \psi_{0y}(x^*, y^*)\cos(\theta)\}\delta_\epsilon(\psi)dxdy \tag{3.16}$$

$$\frac{\partial r}{\partial t} = \int_\Omega S(\phi, \psi)\{-\psi_0(x^*, y^*) + \psi_{0x}(x^*, y^*)x^* + \psi_{0y}(x^*, y^*)y^*\}\delta_\epsilon(\psi)dxdy \tag{3.17}$$

$$\frac{\partial \theta}{\partial t} = \int_\Omega S(\phi, \psi)\{-r\psi_{0x}(x^*, y^*)y^* + r\psi_{0y}(x^*, y^*)x^*\}\delta_\epsilon(\psi)dxdy \tag{3.18}$$

where

$$\psi_{0x} = \frac{\partial \psi_0}{\partial x}, \quad \psi_{0y} = \frac{\partial \psi_0}{\partial y}$$

and (x^*, y^*) is defined according to (3.12).

Gaussian filtering is applied to regularize functions ϕ and ψ at each iteration to achieve a smooth level set function and shape. The algorithm for solving $E(\phi, \psi)$ is given in Table 3.3.

Table 3.3: Method for solving $E(\phi, \psi)$.

A) **Definitions**:

I_0 : Initial image to segment

ψ_0 : Given shape

ψ : Transformed shape given by (3.12)

ϕ : Level set function for segmentation

L : Labeling function

β : Parameter weight of the shape term

α : Parameter for intensity inhomogeneity

G_γ : Gaussian filtering with standard deviation γ

t : Step size

B) **Set initial conditions**:

Initialize ϕ at $t = 0$ as $\phi(x, t = 0) = \begin{cases} \omega & \text{if } x \in \Omega \setminus \Omega_0 \\ 0 & \text{if } x \in \partial\Omega_0 \\ -\omega & \text{if } x \in \Omega_0 \setminus \partial\Omega_0 \end{cases}$

where $\omega > 0$ is a constant, Ω_0 is a subset of Ω and
$\partial\Omega_0$ is the boundary of Ω_0.
Labeling function L is set to either $+1$ and -1 depending on
whether the prior shape is enforced or not.

C) **For** $n : n = 1, 2, \ldots$

1) Compute c_1 and c_2 by (3.6)

2) Evolve the level set function ϕ according to (3.14).

3) At each iteration, update ψ function using (3.15)-(3.18).

4) Evolve the level set function ϕ according to (3.14).

5) Regularize the level set function ϕ and ψ using the Gaussian kernel,
i.e., $\phi = G_\gamma * \phi$,$\psi = G_\gamma * \psi$, where γ is the standard deviation.

6) Check whether the evolution is stationary. If not, return to Step 2.

Chapter 4

Experimental results

In this section, we illustrate the experimental results of our proposed method. We tested our model on noisy, occluded, and low-contrast images, with varying parameters. The scale parameter σ defines the size of the kernel K_σ; its value depends on the image content. If σ is too small, we cannot segment the desirable objects. In contrast, if σ is too large, it may result in high computational costs. For the Gaussian filtering G_γ, γ is chosen between 0.5 and 1, and the kernel size is 5×5.

Figures 4.1, 4.2 and 4.3 show the result of the first case of the proposed model, i.e., the prior shape is placed exactly at the locations of desired objects. Figures 4.4, 4.5, 4.6 and 4.7 show the results of the second case, i.e., the prior shape is placed at arbitrary locations. In Fig.4.1, we utilize our algorithm for a synthetic image in the cases of no prior shape, including the prior shape, and with noise. Our segmentation model works well for each of these cases when some parts are missing as shown in the Figs4.1(c) and (d). For the synthetic image, we set $\sigma = 3$, $\gamma = 0.65$ to regularize the level set, the time step $\Delta t = 0.005$, and $\alpha = 0.0005$ for the global image fitting term.

We also tested our algorithm on real images with shape information as shown in Fig.4.2. As demonstrated in Fig.4.2(a), if no shape prior is given, the algorithm cannot extract the object. However, when shape prior information

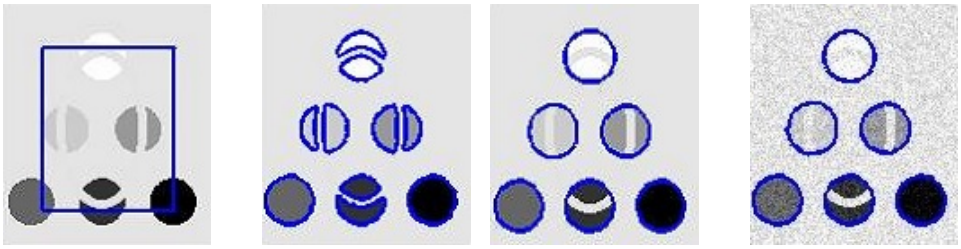

(a) (b) (c) (d)

Figure 4.1: Segmentation results of the proposed model:(a) given image with initial level set, (b) result without shape prior, (c) result with shape prior, (d) result in the presence of noisy.

is used, the model segments the desired objects, even when image is occluded as shown in Figs.4.2(b),(c), and (d). Figure 4.2(c) illustrates the result when the labeling function L is not incorporated in the model.

The comparison of the first case of our model to the extension of Cremers et al.'s model is shown in Fig.4.3. Figures 4.3(b) and (c) show the extension of Cremers et al.'s model using two level set functions and two labeling function to segment occluded and corrupted objects. Our proposed model can segment these objects using only one level set function as shown in Fig.4.3(d).

For the implementation of the second case of our model, we set the translation parameter $(a, b) = (0, 0)$ to be the origin of the plane. We tested the image in Figs.4.4(a) and (b) using the Chan-Zhu model. We also tested this image using our proposed method. As seen in Figs.4.4(c) and (d), the hand and other objects are segmented correctly using only one level set function.

In Fig.4.5, the intensity of the object in the given image is similar to the background intensities. As seen in Fig.4.5(b), the modified LIF and Chan-Vese algorithms are unable to segment the hand in the given image. By utilizing shape information and the second case of our model, the results in Figs.4.5(c) and (d) are obtained. Although, the object is successfully extracted, the value of σ is large, which may cause high

computational costs. Computational time and costs are shown in Table 4.1. If the Chan-Zhu model is used to extract the hand in the image using the same shape prior(see Fig.4.5(e)) as in Fig.4.5(a), the hand cannot be extracted either (Fig.4.5(f)). In other words, the Chan-Zhu model works well when the prior shape is placed near the object. This is illustrated by the next example as well.

Finally, we applied the proposed model to a brain image to extract the corpus callosum. We compared our model with the extensions of Cremers et al.'s model and Chan-Zhu's model. The shape of the corpus callosum is placed arbitrary locations. As shown in Figs.4.6(b) and 4.6(d), the proposed model successfully extracts the corpus callosum in brain image. Our model permits the shape prior to be placed far from the desired objects whereas Chan and Zhu's model requires the initial prior shape to be close to the desired object. In other words, the Chan-Zhu model is not as accurate as our proposed model. These results are shown in Figs.4.7(c) and 4.7(d). Table 4.1 shows the comparison of computation time of our model to other models.

Table 4.1: Computation time results.

Methods	Bird	Hand	Corpus callosum
	Iter(Time(s))	Iter(Time(s))	Iter(Time(s))
4 phase Cremers	50(25.51)	-	300(49.81)
Chan-Zhu model	-	50(94.63)	90(158.72)
Proposed method	200(2.79)	60(23.24)	200(2.46)

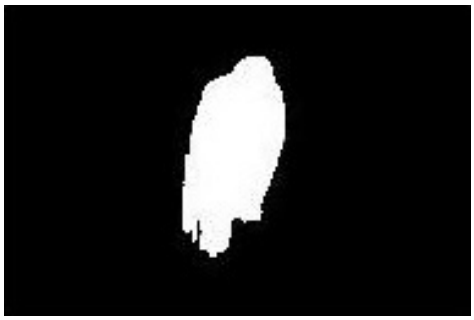

(a)

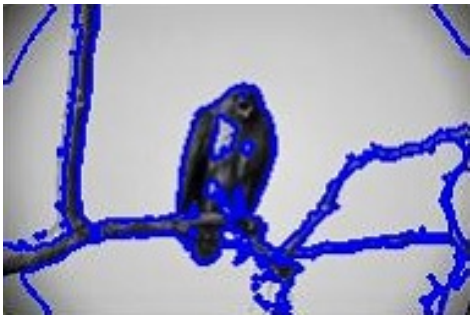

(b)

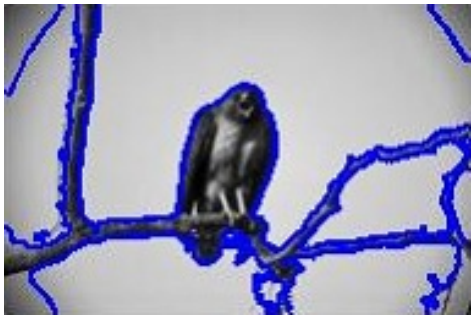

(c)

(d)

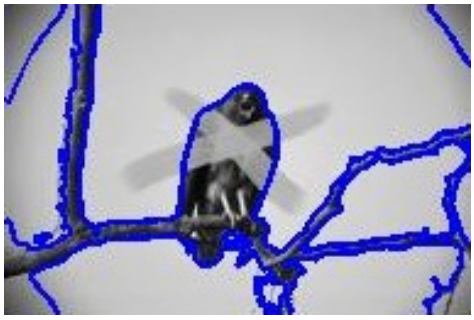

(e)

Figure 4.2: Segmentation results of the proposed model: (a) given shape, (b) result without shape prior, (c) result with shape prior, (d) result without labeling function L, and (e) result with labeling ($\sigma = 6, \gamma = 0.5$).

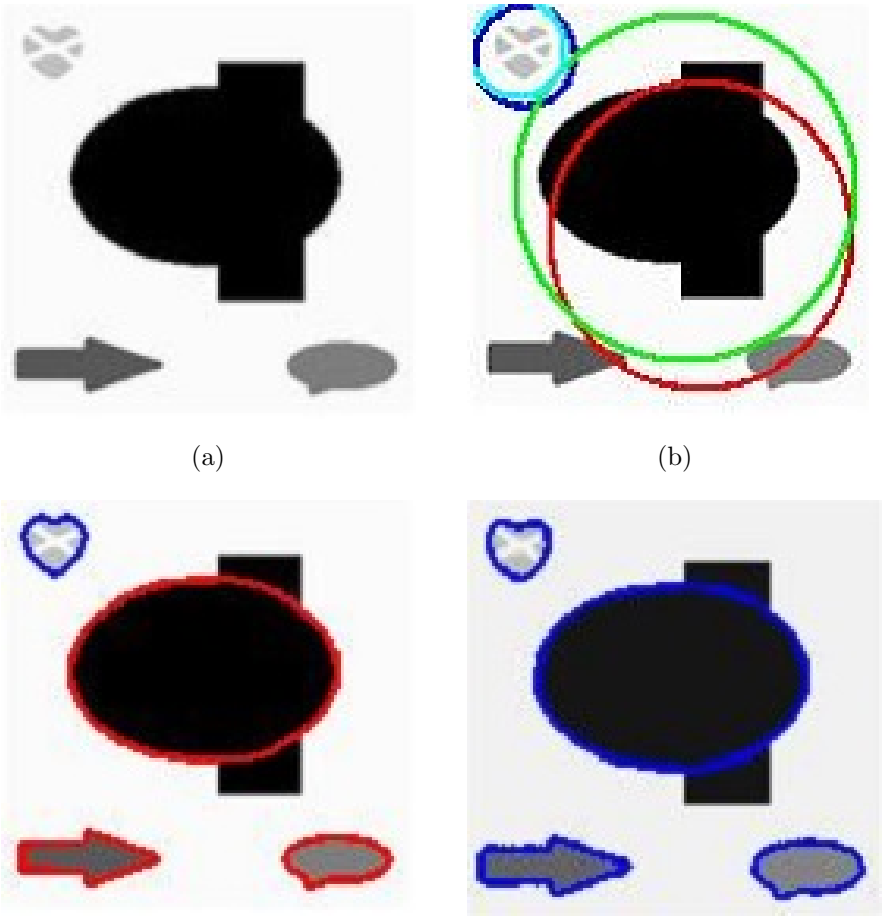

(a) (b)

(c) (d)

Figure 4.3: Segmentation results of the proposed model: (a) original synthetic image, (b) initial ϕ_1 (blue) and ϕ_2 (red) and labeling functions L_1-sky blue, L_2-green, (c) result of the four phase Cremers et al.'s model, and (d) result of the proposed model.

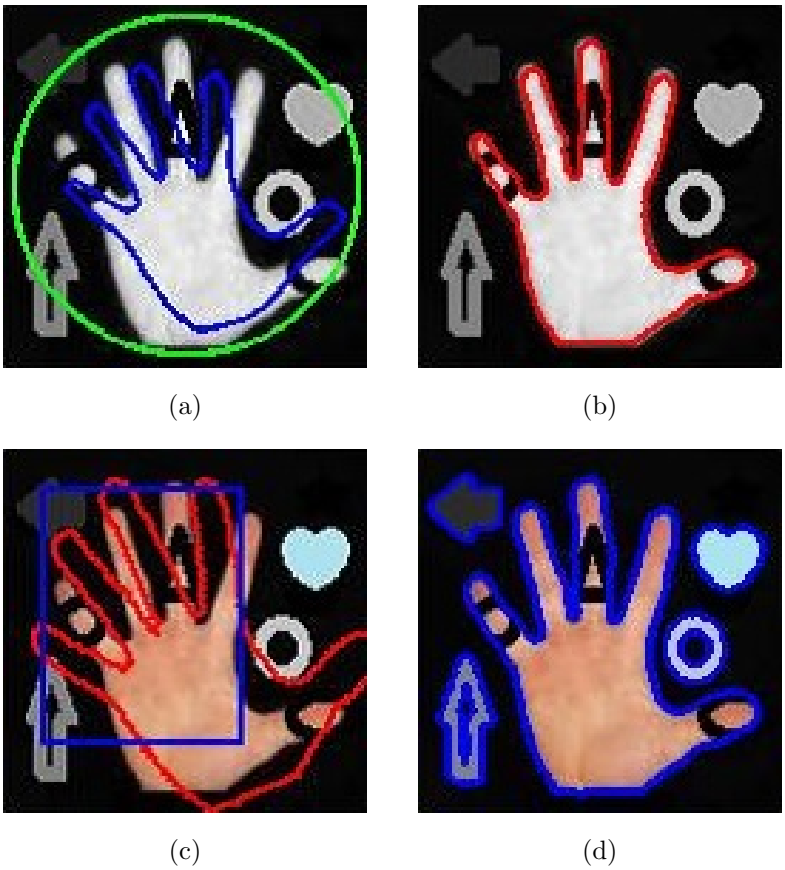

(a) (b)

(c) (d)

Figure 4.4: Segmentation results of the proposed model: (a) original image with initial shape superimposed under the Chan-Zhu model, (b) segmentation result of the Chan-Zhu model, (c) original image with initial shaped superimposed, and (d) segmentation result of the proposed model.

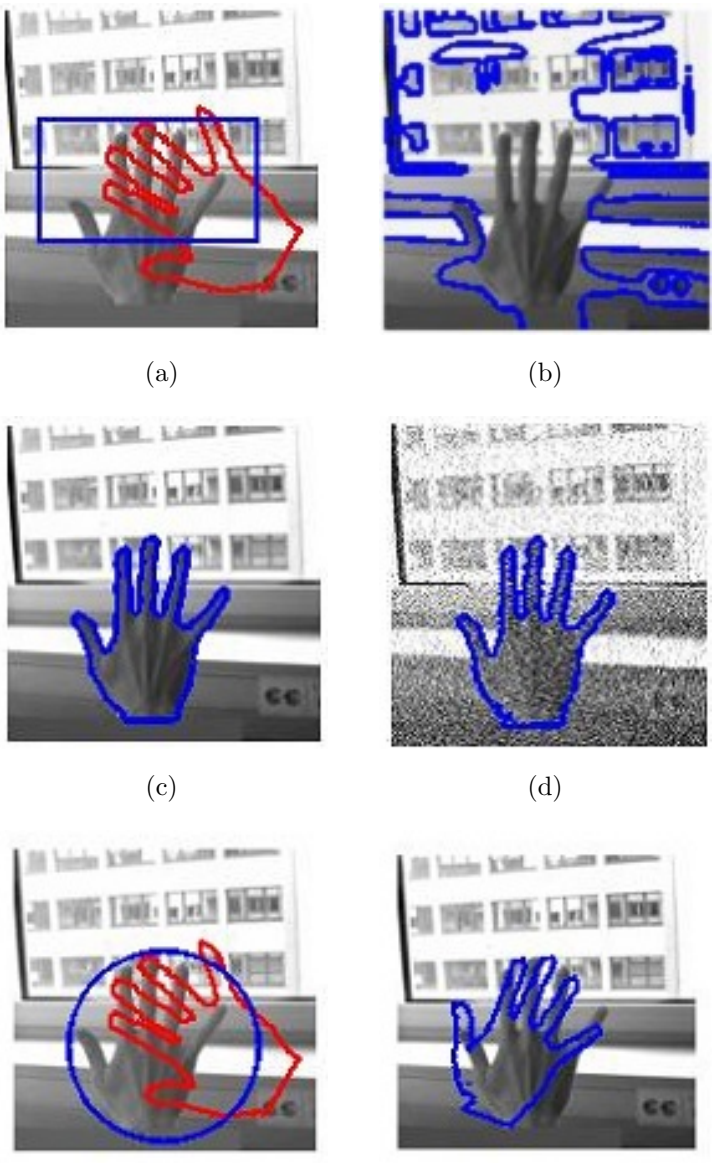

(a) (b)

(c) (d)

(e) (f)

Figure 4.5: Segmentation results of the proposed model: (a) initial ϕ and shape ψ, (b) result without shape prior, (c) result with shape prior ($\sigma = 60, \gamma = 0.5$), (d) result in presence of Gaussian noise ($\sigma = 60, \gamma = 0.9$), (e) initial level set of the Chan-Zhu model, and (f) result of the Chan-Zhu model.

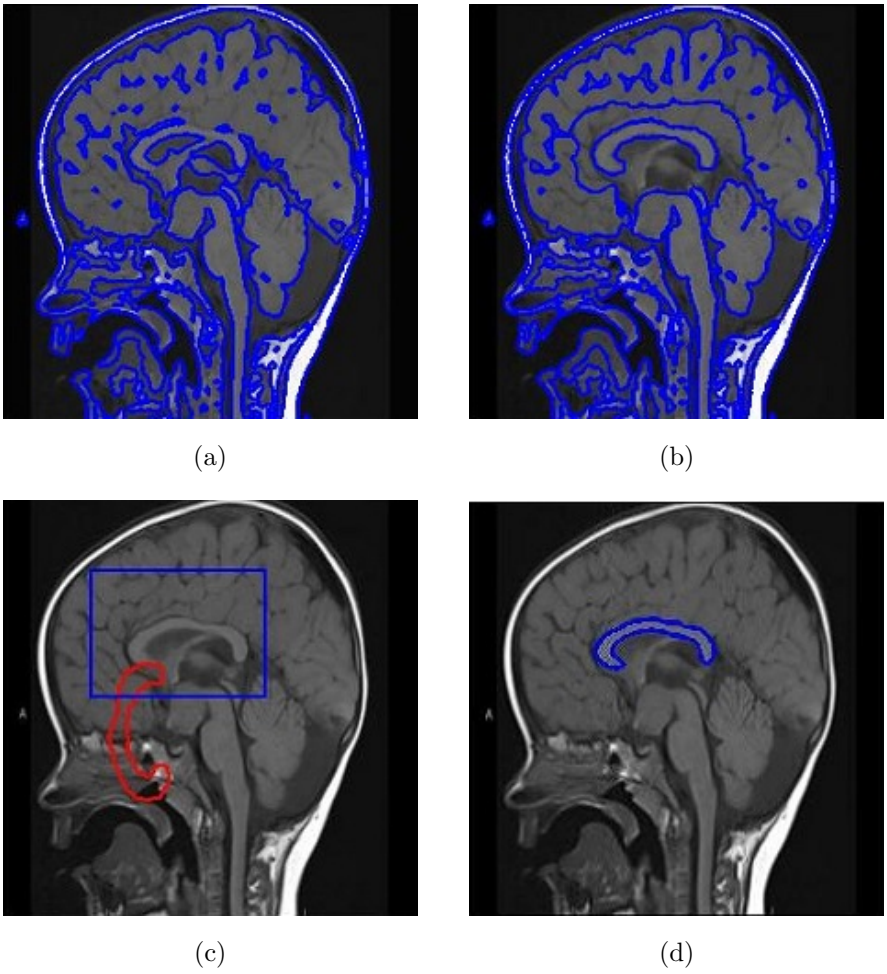

(a) (b)

(c) (d)

Figure 4.6: Segmentation results of the brain:(a) without shape prior, i.e., result of the modified LIF model, (b) result of the proposed model with labeling function ($\sigma = 3, \gamma = 0.5$), (c) initial ϕ and shape ψ for the proposed model, and (d) result of the proposed model without labeling.

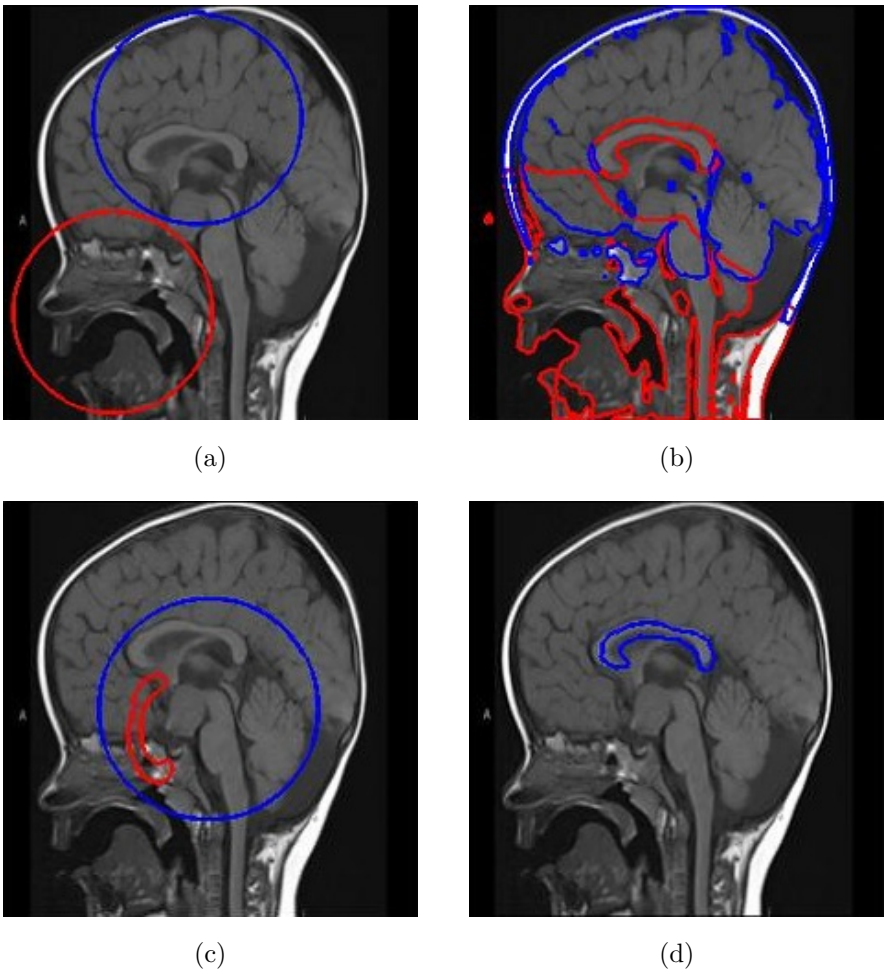

(a) (b)

(c) (d)

Figure 4.7: Segmentation results of the brain: (a) initials ϕ_1(red) and ϕ_2(blue) for the four-phase Cremers et al.'s model, (b) result of the four-phase Cremers et al's model, (c) initial ϕ and shape ψ for the Chan-Zhu model, and (d) result of ψ for the Chan-Zhu model.

Chapter 5

Conclusion

We proposed the global and local image fitting energy method for images with intensity inhomogeneity. In order to cope with the intensity inhomogeneity of the image, we set a local image fitting term. To overcome initialization sensitivity, a global image fitting term was considered. Our segmentation results were obtained faster, requiring fewer iterations than the LBF, LGIF and LIF models. Moreover, our method worked well for multiple objects with varying intensities and allowed flexible initialization of the contours. We also proposed a new method for shape prior segmentation, called the global and local image fitting energy with shape prior. For the shape prior segmentation method, we considered two cases: when prior shapes were placed exactly at the locations of the desired objects and when they were placed at arbitrary locations.

Our model has many advantages over Cremers at el.'s model. First, our model can segment objects using only one level set function, while two level set functions are required by the four phase case of Cremers et al.'s model. In particular, our model can segment multiple objects with different intensities using only one level set function, even when a given image is corrupted. Second, our method is simple, cheaper and faster. Computationally speaking, our method is easier to numerically compute and takes less time to implement. Third, the transformation of prior shape

is not dependent on the locations of the shape and its size.

There are a few disadvantages of our model, however. In our model, it is possible for prior shape to be selected by a similar object rather than the training shape. In particular applications, the prior shape ψ_0 has to be embedded as the mean shape of a set of training shape; for the corpus callosum case, the training shape of their shapes must be used. Furthermore, our method cannot represent triple junctions because it only uses one level set function. In the future, we will work to overcome these drawbacks and also plan to extend our method to multi-phase level set formulation.

Bibliography

[1] D. Mumford and J. Shah, *Optimal approximation by piecewise smooth functions and associated variational problems*, Comm. Pure Appl. Math., 42:577–685, 1989.

[2] T. Chan and L. A. Vese, *Active contours without edges*, IEEE Trans. Image Proc., 10:266–277, 2001.

[3] S. Osher and J. A. Sethian, *Fronts propagating with curvature dependent speed: algorithms based on Hamilton-Jacobi formulations*, J. Comput. Phys., 79:12–49, 1988.

[4] L. A. Vese. and T. Chan, *A multiphase level set framework for image segmentation using the Mumford and Shah model*, International Journal of Computer Vision, 50(3):271–293, 2002.

[5] M. Leventon, W. Grimson, and O. Faugeraus, *Statistical shape influence in geodesic active contours*, CVPR., 316–323, 2000.

[6] D. Cremers, F. Tischhauser, J. Weickert, and C. Schnorr, *Diffusion snakes: introducing statistical shape knowledge into the Mumford-Shah functional*, Int. Journal of Computer Vision, 50(3):295–313, 2002.

[7] D. Cremers, T. Kohlberger, and C. Schnorr, *Shape statistics in kernel space for variational image segmentation*, Pattern Recognition, 36(9): 1929–1943, 2003.

BIBLIOGRAPHY

[8] Y. Chen and H. D. Tagare, *Using prior shapes in geometric active contours in variational framework*, International Journal of Computer Vision, 50(3): 315–328, 2002.

[9] D. Cremers, N. Sochen and Ch. Schnorr, *Towards recognition-based variational segmentation using shape priors and dynamic labeling*, Int.Conf. on Scale Space Theories in Computer Vision, 2695: 388–400, 2003.

[10] T. Chan. and W.Zhu, *Level set based shape prior segmentation*, IEEE Conference on Computer Vision and Pattern Recognition, 2: 1164–1170, 2005.

[11] C. M. Li, C. Kao, J. Gore and Z. Ding, *Implicit active contours driven by local binary fitting energy*, IEEE Conference on Computer Vision and Pattern Recognation, 2007.

[12] C. M. Li, C. Kao, J. Gore and Z. Ding, *Minimization of region-scalable fitting energy for image segmentation*, IEEE Transaction on Image Processing 17: 1940–1949, 2008.

[13] L. Wang, C. Li, Q. Sun, D. Xia and C. Kao, *Brain MR image segmentation using local and global intensity fitting active contours/surfaces*, Proc. Medical Image Computing and Computer Aided Intervention (MICCAI),Part I, 5241: 384–392, 2008.

[14] K. Zhang, H. Song and L. Zhang, *Active contours driven by local image fitting energy*, Pattern Recognation, 43(4): 1199-–1206, April 2010.

[15] J. A. Sethian, *Level set methods and fast marching methods*, Cambridge: Cambridge University Press, 1999.

[16] V. Caselles, F. Catte, T. Coll, and F. Dibos, *A geometric model for active contours in image processing*, Numer. Math., 66: 1–31, 1993.

[17] V. Caselles, R. Kimmel, and G. Sapiro, *Geodesic active contours*, Intl J. Comp. Vis., 22: 61–79, 1997.

[18] R. Malladi, J. A. Sethian, and B. C. Vemuri, *Shape modeling with front propagation: a level set approach*, IEEE Trans. Patt. Anal. Mach. Intell., 17: 158–175, 1995.

[19] M. Kass, A. Witkin and D. Terzopoulos, *Snakes: active contour models*, Int.J. Comput. Vision, 1: 321–331, 1988.

[20] S. Osher, and R. Fedkiw, *Level set methods and dynamic implicit surfaces*, Springer-Verlag, New York, 2002.

[21] G. Russo and R. Smereka, *A remark on computing distance functions*, J.Comput.Physics, 163: 51–67, 2000.

[22] D. Peng, B. Merriman, S. Osher, H. Zhao, and M. Kang, *A PDE-based fast local level set method*, J.Comp.Phys., 155: 410–438, 1999.

[23] M. Sussman, P. Smereka, and S. Osher, *A level set method for computing solutions to incompressible two-phase flow*, J.Comp.Phys., 127: 179–195, 1996.

[24] T. F. Chan and L. A. Vese, *Image segmentation using level sets and the piecewise constant Mumford-Shah model*, Tech. Rep. CAM 00-14, UCLA Dep. Math, 2000.

[25] Y. Chen, H. D. Tagare, S. Thiruvenkadam, F. Huang, D. Wilson, K. S. Gopinath, R. W. Briggs, and E. A. Geiser, *Using prior shapes in geometric active contours in a variational framework*, International Journal of Computer Vision, 50(3): 315–328, 2002.

[26] Y. Chen, S. Thiruvenkadam, H. D. Tagare, F. Huang, D. Wilson, and E. Geiser, *On the incorporation of shape priors into geometric active contours*, In Variational and Level Set Methods in Computer Vision, 145–152, 2001.

[27] S. R. Thiruvenkadam, T. F. Chan, and B. W. Hong, *Segmentation under occlusions using selective shape prior*, SSVM, 4485: 191–202, 2007.

[28] J. Woo, P. J. Slomka, C. C. Jay Kuo and B. W. Hong, *Multiphase segmentation using an implicit dual shape prior: application to detection of left ventricle in cardiac MRI*, Computer vision and Image Understanding 117: 1084–1094, 2013.

[29] T. Cootes, and C. Taylor, *Statistical models of appearance for computer vision*, University of Manchester, Wolfson Image Analysis Unit, Imaging. Sci and Biomedical. Eng., 48–69, 1999.

[30] T. F. Cootes, C. J. Taylor, D. H. Cooper and J. Graham, *Active shape models: their training and application*, Computer Vision and Image Understanding, 61(1): 38–59, 1995.

[31] X. Bresson, P. Vandergheynst and J. P. Thiran, *A variational model for object segmentation using boundary information and shape prior driven by the Mumford-Shah functional*, International Journal of Computer Vision, 68(2): 145–162, 2006.

[32] N. Paragios, M. Rousson and V. Ramesh, *Matching distance functions: a shape-to-area variational approach for global-to-local registration*, ECCV, Copenhangen, Denmark, 2002

[33] M. Rousson and N. Paragios, *Shape priors for level set representations*, ECCV, Copenhangen, Denmark, 2002.

[34] A. Tsai, A. Yezzi, W. Wells, C. Tempany, D. Tucker, A. Fan, W. E. Grimson and A. Willsky, *A shape-based approach to the segmentation of medical imagery using level sets*, IEEE Trans.Med.Imag., 22(2): 137–154, 2003.

[35] A. Yezzi, A. Tsai and A. Willsky, *A statistical approach to snakes for biomodal trimodal imagery*, Int. Conf. on Comput. Vis., 898–903, 1999.

BIBLIOGRAPHY

[36] C .M. Li, C. Y. Xu, C. F. Gui and M. D. Fox, *Level set evolution without re-initialization: a new variational formulation*, IEEE Conference on Computer Vision and Pattern Recognation, San Diego, 430–436, 2005.

[37] C. M. Li, C. Y. Xu, C. F. Gui and M. D. Fox, *Distance regularized level set evolution and its application to image segmentation*, IEEE Transactions on Image Processing, 19(12), 2010.

[38] H. K. Zhao, T. Chan, B. Merriman and S. Osher, *A variational level set approach to multiphase motion*, JCP., 127: 179–195, 1996.

[39] G. Aubert and P. Kornprobst, *Mathematical problems in image processing, PDEs and the calculus of variations*, Second Edition, Springer Science, 2006.

[40] S. Kim, and M. Kang, *Multiple-region segmentation without supervision by adaptive global maximum clustering*, IEEE Transactions on Image Processing, 21: 1600–1612, 2012.

[41] Z. Hou, *A review on MR image intensity inhomogeneity correction*, Int. J. Biomed. Img., 2006.

[42] R. Fahmi and A. Farag, *A fast level set algorithm for shape-based segmentation with multiple selective priors*, Proc. of IEEE International Conference on Image Processing, San Diego, California, October 12–15, 2008.

국문초록

이 논문에서 우리는 형태 사전 지식을 사용한 레벨 셋 방법에 기초해서 분할 알고리즘을 다룬다. 기본적인 분할 모델은 대상이 가려져 있거나 일부분이 누락된 경우에 배경에서 바람직한 대상을 분할하지 못한다. 이런 어려움을 극복하기 위해서 부분 및 전체 이미지 정보를 이용해서 만든 에너지 함수를 형태 사전 지식과 통합한다. 이 방법은 다른 문헌에서 제시된 방법들을 향상 시켜서 심지어 이미지가 누락돼있거나 가려짐, 잡음, 낮은 명암을 가진 불균일한 강도의 이미지도 분할한다. 우리는 두 가지 경우를 고려한다. 하나는 형태 사전 지식이 원하는 개체의 위치에 정확하게 배치되고, 다른 하나는 형태 사전 지식이 임의의 위치에 배치된다. 우리는 다양한 이미지에 우리 방법을 테스트하고 기존의 다른 방법과 비교한다. 실험 결과들로 우리 방법이 정확하고 계산이 효율적일뿐만 아니라 기존의 방법들보다 더 빠르다는 것을 볼 수 있다.

주요어휘: 분할, 적극적 경로, 형태 사전 지식, 레벨 셋 방법, 강도의 불균일성
학번: 2010-31290